A quasi-dynamic air traffic assignment model for mitigating air traffic complexity and congestion for high-density UAM operations

Zhengyi Wang, Daniel Delahaye, Jean-Loup Farges, Sameer Alam

A quasi-dynamic air traffic assignment model for mitigating air traffic complexity and congestion for high-density UAM operations

Zhengyi Wang[a,c,*], Daniel Delahaye[a], Jean-Loup Farges[b], Sameer Alam[c]

[a] *OPTIM Group, ENAC Lab, Ecole National de l'Aviation Civile, Toulouse, France*
[b] *ONERA, Toulouse, France*
[c] *ATMRI, Nanyang Technological University, Singapore*

Abstract

In spite of the significant effects of COVID-19, UAM operations are still expected to grow smoothly and healthily in the near future. If such dense UAM traffic relies on tactical planning to resolve conflicts in a decentralized control scheme, urban airspace could soon be heavily congested and airspace complexity could be overwhelming. In this paper, we propose a Quasi-dynamic Air Traffic Assignment (QATA) model, which aims to allocate traffic flows among air routes in the planning horizon in order to organize UAM traffic flows and reduce air traffic congestion and complexity within a centralized strategic planning scheme while meeting the demand and respecting some criteria. Firstly, UAM traffics are modeled as flows that operate on a 3D two-way UAM route network. Next, the QATA problem is formulated as an optimization problem involving network dynamics to minimize the air traffic complexity evaluated by the linear dynamical system and congestion defined by traffic density and energy consumption. A simulation-based rolling horizon framework is introduced to decompose the QATA problem into several modified static air traffic assignment problems in each time interval. In order to overcome the limitations of conventional dynamic traffic assignment algorithms, a simulated annealing algorithm using parallel computing and a novel neighborhood generation strategy is proposed to efficiently optimize the problem. By applying the model to a pre-designed large-scale UAM route network in Singapore's urban airspace, Experimental studies demonstrate the performance of the proposed framework and its applicability. Parallel computing can achieve up to three times faster than the original algorithm. The proposed algorithm significantly reduces the value of the objective function by $(32.20 \pm 0.29)\%$ in 143.47 ± 3.74 seconds at the 95% confidence interval of 100 experiments, far better compared to the representative conventional dynamic traffic assignment algorithms. This study could be useful to assist air traffic control authorities and air navigation service providers in addressing various issues in unmanned traffic management.

Keywords: Urban Air Mobility, Unmanned Traffic Management, Air traffic Assignment, Air Traffic Complexity, Unmanned aerial vehicle, Air traffic flow management

1. Introduction

Urban Air Mobility (UAM) offers on-demand or scheduled air transport services within metropolitan areas. This concept employs unmanned and manned aerial vehicles for cargo or passenger carrying with high automation. Despite the huge impact of COVID-19 lasting more than two years, UAM operations are expected to grow smoothly and healthily on a global scale in recent years (FAA, 2020a, Chen et al., 2022). Balakrishnan et al. (2018) estimates that for a metropolis such as Paris, the demand for UAM vehicles for deliveries could be as high as 8,333 per hour by 2035. Doole et al. (2020) even made a nearly eight-fold forecast for the same scenario. However, congestion in the urban environment is growing steadily while available airspace remains roughly the same. To this end, various industry (Singireddy and Daim, 2018, Lascara et al., 2019), academia (Low et al., 2014, Doole et al., 2021), and government-led (FAA, 2020b, Jang et al., 2017, Geister, 2017, Sunil et al., 2015) initiatives have been developed to integrate UAM operations into the current air transportation system. These projects aim to minimize negative impacts on existing ATM systems by structuring UAM operations in constrained low-altitude urban areas, such as class G airspace (Bauranov and Rakas, 2021). The airspace is further segmented into several altitude layers, and UAM vehicles are expected to operate in fixed route structures and follow the corresponding procedures, rules, and performance requirements.

Similar to Air Traffic Management (ATM), Unmanned Traffic Management (UTM) can be divided into four stages: airspace organization and management, air traffic flow management, separation provision, and collision avoidance, ranging from the most preventive to the most reactive level. The first two elements involve strategic planning, which has a long look-ahead time, whereas the last two elements are part of tactical planning that involves measures with short-term effects. When the density of UAM operations reaches a high level, strategic planning is required to organize the airspace and manage the air traffic flow with the support of automated UAM operations on a highly-integrated UAM route network (Hill et al., 2020, Evans et al., 2021, Ng, 2020). In addition, strategic planning could also ease the pressure on tactical planning stages and increase the overall safety, efficiency, capacity, and predictability of the air transportation system.

The architecture of the UTM system can be broadly classified into three categories: decentralized, centralized, and federated. In the decentralized architecture, each Provider of Services for UAM (PSU) assumes responsibility for managing a group of UAVs within its designated airspace by providing conflict resolution services, which rely on autonomous and distributed data exchange between PSUs. This architecture is currently the most widely used in industrial applications as it allows aircraft to select their preferred routes and maintain safety through the use of tactical collision avoidance systems, such as sense-and-avoid (Yu and Zhang, 2015). The federated architecture of the UTM system combines both decentralized and centralized features (Patterson et al., 2021). It enables distributed data exchange among different entities, with multiple UTM service providers responsible for managing UAVs within their designated airspace. The centralized architecture of the UTM system is characterized by a single PSU with a centralized control center that is responsible for managing all UAVs within the urban airspace by collecting, processing, and disseminating relevant information to all UAVs involved. This study specifically focuses on the centralized UTM system, as it has been suggested that centralized UTM systems offer significant advantages for high-density and complex UAM operations in densely populated metropolitan areas, particularly during the strategic planning phase (FAA, 2020b, Prevot et al., 2016, Goodrich and Barmore, 2018). It is important to emphasize that not all aspects and phases of this UTM architecture require centralization. While air traffic flow management in the strategic planning phase benefits from centralization, other functions such as information sharing, geo-awareness, fleet management, and conflict detection and resolution can be provided in decentralized or federated ways. In addition, the needs, scalability, requirements, and regulations of different regions or areas may vary, leading to the adoption of diverse UTM approaches. Consequently, the architecture of future UAM applications may involve a combination of decentralized, federated, and centralized UTM systems (Bauranov and Rakas, 2021). This approach allows for flexibility and adaptability in UTM operations, as different components can be tailored to specific needs and implemented using the most suitable architecture.

*Corresponding author

Email addresses: zhengyi.wang@ntu.edu.sg (Zhengyi Wang), delahaye@recherche.enac.fr (Daniel Delahaye), jean-loup.farges@onera.fr (Jean-Loup Farges), sameeralam@ntu.edu.sg (Sameer Alam)

As a strategic planning model deployed in centralized systems, air traffic assignment turns out to be a key aspect in designing new operation concepts and supporting automated decision-making in UAM. It refers to a broad optimization term related to routing and flow control in air transportation systems (Delahaye and Puechmorel, 2013a). The first model of air traffic assignment is developed as early as in 1954. This model addressed the assignment for a given fleet to carry an anticipated traffic load over several routes at the minimum cost. Since then, a variety of traffic assignment models have been developed for solving routes and slot allocation problems (Farges and Delahaye, 2001, Deschinkel et al., 2002, Delahaye et al., 2005, Nosedal et al., 2014), air traffic flow management (Strub and Bayen, 2006, Bertsimas et al., 2011, Zhang et al., 2012, 2015), en-route network management (Delahaye and Puechmorel, 2013b, Haouari et al., 2009), etc. Some other air traffic assignment studies have been carried out for different purposes, including noise reduction (Netjasov, 2008, Ganić et al., 2018, Chatelain and Van Vyve, 2018, Ho-Huu et al., 2019), and emission reduction (Economou et al., 2007, Mirosavljević et al., 2011, Ho-Huu et al., 2019). In the context of UTM, most research has focused on UAV task assignment (Jiang et al., 2017, Zhou et al., 2018, Cheng et al., 2019, Liu et al., 2019). Nevertheless, a majority of previous research dealt with individual aircraft from a microscopic perspective. For high-density UAM traffic, the Eulerian approach, which focuses on analyzing aggregate measures and characteristics of traffic flow as a whole, is preferred over the Lagrangian approach of tracking individual trajectories (Bombelli, 2017). Given the uncertainty of actual take-off times during planning and the challenges of tracking each trajectory, the Eulerian perspective provides a macroscopic view of traffic flow, considering overall patterns and congestion levels. While the Lagrangian approach is capable of addressing current real-world problems, it can pose challenges due to computational complexity and calibration difficulties when envisioning future scenarios where the quantity of UAM aircraft in urban airspace may differ significantly from the existing number of aircraft (Mollier et al., 2019).

To provide a comprehensive evaluation of the level of disorder in the UAM route network, it becomes essential to aggregate the dynamics of individual vehicles into the air traffic flow to gain insights into the overall flow characteristics. In terms of aggregate measures, Congestion is an important estimator of traffic conditions. However, it is highly correlated with traffic density. Without involving traffic dynamics, the congestion reveals only partial information about the traffic condition. For example, in a ground-based Air Traffic Control (ATC) system, air traffic controllers may continue to accept structured air traffic flow when airspace capacity is exceeded but may refuse disordered air traffic even if the capacity threshold is not reached (Delahaye and Puechmorel, 2013a). It is well established that the disorder of traffic situation is ultimately associated with the difficulty and effort of managing air traffic in the specified airspace (Prandini et al., 2011). This term is defined as air traffic complexity, which is an intrinsic measure involving the dynamic of air traffic, independent of airspace structure and ATC systems. Numerous air traffic complexity metrics have been explored, including convergence metric (Delahaye and Puechmorel, 2000), geometric metric (Delahaye and Puechmorel, 2000), proximity metric (Delahaye and Puechmorel, 2000), clusters metric (Histon et al., 2002, Koca et al., 2019), Grassmannian metric (Delahaye and Puechmorel, 2013c), König metric (Essén, 1993, Delahaye et al., 2002, Juntama et al., 2020), collision metric (Radanovic et al., 2018), graph-based metric (Isufaj et al., 2022), optimal control-based metrics (Lee et al., 2007), machine learning-based metrics (Zhang et al., 2021), etc. Although these metrics have been demonstrated to be effective in typical traffic situations, most metrics are not designed for complex and dense traffic. In addition, the spatial-temporal information is not taken into account in many of the previous works. To address these challenges, Linear Dynamical Systems (LDS) is introduced in this study to measure the complexity of air traffic and has been successfully applied in many studies (Delahaye and Puechmorel, 2000, Delahaye et al., 2002, 2004, Delahaye and Puechmorel, 2010, Treimuth et al., 2015, Juntama et al., 2022). With a strong theoretical framework, LDS evaluates the air traffic complexity by describing the evolution of a given traffic situation. It is able to efficiently quantify the level of disorder and interaction between a large number of aircraft.

The route choice of each traveler is influenced by the route condition of the UAM network, which in turn is determined by the route choices and flow patterns observed at different time intervals (Chiu et al., 2011). To determine the optimal traffic flow pattern in traffic assignment, a two-step process is required (Ameli et al., 2020a): (1) Constructing the route network by identifying feasible paths between Origin-Destination (OD) pairs, and (2) Calculating the optimal path flow based on demand and network dynamics. Previous studies by the authors (Wang et al., 2021, 2022a,b) have contributed to both steps. For the first step,

Wang et al. (2022a) developed a methodology to design route networks for future UAM operations, aiming to minimize noise impact while maximizing flight safety and efficiency. On the other hand, Wang et al. (2021) and Wang et al. (2022b) focused on the second step by decreasing the intrinsic air traffic complexity of UAM operations. Wang et al. (2021) introduced a Static Air Traffic Assignment (SATA) model for 2D UAM transport networks and proposed a hybrid algorithm based on Dafermos' Algorithm (DA) to optimize the problem. Wang et al. (2022b) extended this work to 3D UAM operations. A two-step algorithm that incorporates Simulated Annealing (SA) and DA is introduced to approximate the optimal solution. However, some assumptions of these models, such as static demand and static network loading, are impractical given the complex and ever-changing traffic conditions. It is crucial to include temporal information in network dynamics. Additionally, these optimization methods were primarily designed for small-scale networks, and their performance may deteriorate when applied to larger networks.

In this paper, we propose a Quasi-dynamic Air Traffic Assignment (QATA) framework to allocate high-density traffic demands, estimated within a planning horizon, to paths between ODs in existing air transportation networks. The goal is to minimize air traffic complexity and congestion. The term *quasi* is due to the fact that the demand is discrete in time. Initially, the UAM route network is represented as a graph, with links modeled as volume segments and nodes representing vertiports, delivery stations, and waypoints. In the centralized control scheme, a QATA problem is formulated to obtain an optimal flow pattern from a macroscopic perspective by structuring the high-density hourly UAM traffic into flows. Traffic dynamics and flow propagation is considered in the model. The objective function consists of the air traffic complexity metric based on LDS and congestion related to flow and energy consumption. To efficiently solve the QATA problem, we propose a simulation-based rolling horizon framework. By decomposing the original problem into several sub-problems, a modified Static Air Traffic Assignment (SATA) problem is addressed. Traditional optimization algorithms used for dynamic traffic assignment, which are based on path-swapping descent direction methods, are often unsuitable for realistic problems lacking an analytical form or involving costly criteria evaluated through complex simulation processes (Ameli et al., 2020a). Moreover, these algorithms do not perform well in larger-scale networks (Patriksson, 2015). To this end, a Parallel Simulated Annealing (PSA) algorithm that utilizes parallel computing and a novel neighborhood generation strategy is introduced to efficiently solve the QATA problem. This study is one of the first attempts to conduct air traffic assignments for dynamic UAM operations from a macroscopic perspective. Based on the previous discussion, the contribution of this paper is summarized as follows:

- a macroscopic formulation of the QATA problem is introduced to handle high-density time-varying demands in future UAM route networks;
- aggregate measurements of air traffic complexity and congestion are modeled based on the intrinsic characteristic of UAM traffic dynamics, flow distribution, and energy consumption;
- within the simulation-based rolling horizon framework, a PSA algorithm using parallel computing and a novel neighborhood generation strategy is developed to efficiently optimize the QATA problem;
- validation of the proposed model through a scenario of parcel delivery service with high-density traffic volume in a large-scale UAM route network in Singapore's urban airspace.

2. Quasi-dynamic air traffic assignment model

2.1. Problem description

NASA developed a framework to measure the UAM Maturity Level (UML) (Goodrich and Theodore, 2021), which is intended to categorize significant phases during the evolution of the UAM transportation system from the current state to a highly developed future state. The problem addressed here focuses on the mature state of UML, which corresponds to high-density and complex UAM operations in a densely populated area. Given time-dependent demands between vertiports and delivery sites, UAM flights are expected to operate as flows from origins to destinations following air routes in the existing UAM route

network in low-altitude urban airspace. The path flow patterns optimized by the QATA model will be provided to operators during the pre-flight planning phase.

The planning horizon is discretized into K equal time intervals. The time-varying demand $D_{w,k}$ refers to the assigned flow on OD pair w at time interval k, which can be obtained in advance from Providers of Services for UAM (PSU) and Supplemental Data Service Provider (SDSP) services (FAA, 2020b).

The UAM route network is modeled as a directed graph $G(\mathcal{V}, \mathcal{E})$ consisting of a set of nodes $\mathcal{V}$ and a set of links $\mathcal{E}$. A node v represents either a waypoint, a vertiport, or a delivery station. Their coordinates are fixed. A link e represents an airway that connects a pair of nodes. All links are directed and can be classified into horizontal links $\mathcal{E}_h$ and vertical links $\mathcal{E}_v$. Furthermore, $\mathcal{E}_v$ includes upward links $\mathcal{E}_u$ and downward links $\mathcal{E}_d$. Let $\mathcal{W}$ be the set of OD pairs. For each OD pair w, we denote $\mathcal{P}_w$ the path set consisting of all feasible paths between w in G.

The main symbols and variables used in the following sections are listed in Table 1.

Table 1: Nomenclature used in this paper.

Term	Description
Air route network	
G	UAM route network
$e \in \mathcal{E}$	A link in the set of links of G
$\mathcal{E}_h, \mathcal{E}_u, \mathcal{E}_d$	Horizontal, upward, and downward links
$v \in \mathcal{V}$	A node in the set of nodes of G
$w \in \mathcal{W}$	An OD pair in the set of OD pairs of G
$p \in \mathcal{P}_w$	A path in the set of feasible paths connecting OD pair w
$\mathcal{U}_e$	UAM volume segment of link e
$\mathcal{A}_v$	Cylindrical airspace around node v
$g \in \boldsymbol{g}_e$	A point in the set of grid points of link e
$\mathcal{Z}_v$	Intersection zone of node v
$\boldsymbol{\gamma}$	Set of proportions for all paths flows in all OD pairs during the planning horizon
$\boldsymbol{\gamma}_{w,k}$	Set of proportions for all path flows in OD pair w in time interval k
$\gamma_{p,k}$	Proportion for path flow in OD of p in time interval k
$\tau_{p,g}$	Free-flow travel time from the origin of a feasible path p to a point $g \in p$
$F_{w_g,p,k}$	Average flow that traverses a grid point g on path p of OD pair w in time interval k
$\hat{F}_{g,k}$	Accumulative path flow on a grid point g in time interval k
$f^{\text{in}}_{e,k}, f^{\text{out}}_{e,k}$	Inflow and outflow of link e in time interval k
f^{c}_{e}	Traffic flow capacity for link e
$D_{w,k}$	Demand of OD pair w in time interval k
$\rho_{g,k}$	Traffic density of point g in time interval k
$s_{e,k}$	Average speed of UAM traffic flow on link e at time interval k
α_e	Energy consumption factor of link e
$\delta_{e,p}$	$= 1$ if link e is contained in path p, otherwise 0
$\delta_{e_g,p}$	$= 1$ if the link e containing grid point g belongs to path p, otherwise 0

2.2. UAM route network modeling

On the basis of the operation volume segment developed by FAA (2020b), each link e in the route network is modeled as 3D blocks of airspace, referred to as UAM volume segment $\mathcal{U}_e$. It is a performance-based 3D route segment consisting of corridors designed to support one-way or two-way point-to-point UAM operations. All UAM vehicles operating within the volume segment should follow specific rules, procedures, and performance requirements with support from the PSUs. The size of $\mathcal{U}_e$ is determined by the performance capabilities of the UTM infrastructure and UAM system. For example, with higher navigational performance, UAM vehicles are allowed to operate in smaller volumes (Decker and Chiambaretto, 2022).

The number of parallel 3D blocks for each UAM segment is denoted as N_s. Figure 1 illustrates an example of two-way UAM volume segments with $N_s = 3$ for a link $e \in \mathcal{E}$ and its inverse link e'. As shown in Figure 1a, each volume segment is composed of several air lanes, which are further divided into grids representing the associated flow information. The center points of grids on a volume segment $\mathcal{U}_e$ are denoted as density points $\boldsymbol{g}_e$, which is illustrated in Figure 1b. Each point $g \in \boldsymbol{g}_e$ is characterized by static properties including coordinate (x_g, y_g, z_g), the direction of velocity θ_g if it belongs to a horizontal link, and dynamic properties in time interval k including average flow speed $s_{g,k}$ and density $\rho_{g,k}$. Thereinto, the θ_g and $s_{g,k}$ correspond with the traffic flow traversing the grid. The grid width is denoted as L_w. Given a predefined standard grid length L_l, the coordinates of density point $\boldsymbol{g}_e$ are calculated from the coordinates of endpoints of the associated link such that all grid length L_g equals L_l except the mid-grid length is in $[L_l, 2L_l[$, as each link cannot be divided equally by L_l. Due to the large differences in the length of horizontal and vertical links, L_l has different values L_h and L_v for horizontal and vertical links, respectively.

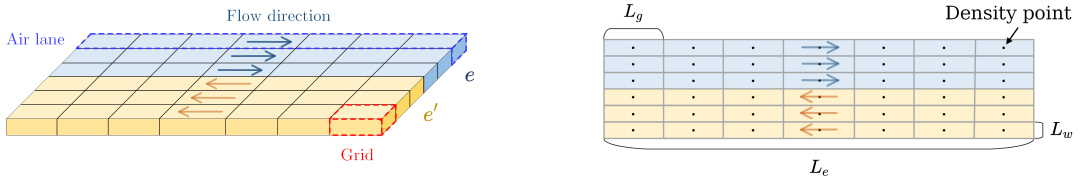

(a) 3D representation of two-way UAM volume segments.

(b) The top view of Figure 1a.

Figure 1: An example of two-way UAM volume segments.

In this study, the amount of air traffic flow distributed per grid segment g during time interval k is defined as the traffic density $\rho_{g,k}$:

$$\rho_{g,k} = \frac{\hat{F}_{g,k}}{s_{g,k}} \tag{1}$$

where $\hat{F}_{g,k}$ is the accumulative path flow on point g and is given later in equation (11).

2.3. Mathematical formulation of QATA problem

2.3.1. Decision variables and constraints

The decision variables in this problem are the proportion of path flow in OD pairs during the planning horizon. Unless otherwise noted, path flow refers to the flow that passes through the origin of a path. Rather than link-based models that require traffic control for each link, the benefit of this formulation is that it can provide accurate path-based flow allocation results, which can facilitate the decision-making process. Such decision variables can be formulated as follows:

$$\boldsymbol{\gamma} = \{\boldsymbol{\gamma}_{w,k} | w \in \mathcal{W}, k = 1, \dots, K\} \tag{2}$$

where

$$\boldsymbol{\gamma}_{w,k} = \{\gamma_{p,k} | p \in \mathcal{P}_w\}, \quad w \in \mathcal{W}, k = 1, \dots, K \tag{3}$$

The decision variables are non-negative and satisfy the conservation law:

$$\gamma_{p,k} \geq 0, \quad p \in \mathcal{P}_w, w \in \mathcal{W}, k = 1, \dots, K \tag{4}$$

$$\sum_{p \in \mathcal{P}_w} \gamma_{p,k} = 1, \quad w \in \mathcal{W}, k = 1, \dots, K \tag{5}$$

Then, the path flow can be derived as:

$$F_{p,k} = D_{w,k} \gamma_{p,k}, \quad p \in \mathcal{P}_w, w \in \mathcal{W}, k = 1, \dots, K \tag{6}$$

The non-zero path flow should be greater than a threshold to make it meaningful for the assignment:

$$F_{p,k} \in \{0\} \cup [F_t, D_{w,k}], \quad p \in \mathcal{P}_w, w \in \mathcal{W}, k = 1, \ldots, K \tag{7}$$

Unlike static formulation, the flow may not traverse a link on a path all the time during a given time interval. To model the propagation of traffic flow, we first introduce the travel time at free-flow conditions from the origin of a feasible path p to a point g on this path:

$$\tau_{p,g} = \sum_{e \in p_g} \frac{L_e}{s_e} + \frac{d(v_g^{\mathrm{f}}, g)}{s_{e_g}}, \quad g \in p, p \in \mathcal{P}_w, w \in \mathcal{W} \tag{8}$$

where p_g is the truncated route segments from the origin of path p to point g, v_g^{f} is the final node of p_g, L_e is the length of link e, s_e is the free flow speed on link e, and e_g is the link containing point g. Figure 2a gives an example for calculating the travel time from the origin of a path to a point g under network representation.

Since $\tau_{p,g} > 0$, then $\exists N \in \mathbb{N}$ and $\tau_\varepsilon \in [0, T_{\mathrm{d}}[$ such that

$$\tau_{p,g} = NT_{\mathrm{d}} + \tau_\varepsilon, \tag{9}$$

where T_{d} is the common duration for all time intervals. The average path flow for a path p on a certain point g during the k-th time interval can be calculated as the weighted average of flows in the previous N-th and $(N+1)$-th time interval uniformly distributed in each corridor, where the weight is linked to the time gap τ_ε:

$$F_{g,p,k} = \frac{1}{N_s}\left[(1 - \frac{\tau_\varepsilon}{T_{\mathrm{d}}})F_{p,k-N} + \frac{\tau_\varepsilon}{T_{\mathrm{d}}}F_{p,k-N-1}\right], \quad p \in \mathcal{P}_w, w \in \mathcal{W}, k = 1, \ldots, K \tag{10}$$

This rationale can be interpreted in Figure 2b, a case $\tau_{p,g} < T_{\mathrm{d}}$. The path flow in time intervals $[t_0, \tau_{p,g}]$, $[t_1, \tau_{p,g}]$, and $[t_2, \tau_{p,g}]$ are flows from previous time steps that cannot be finished. Thus the average path flow on a point g in each time interval has to be calculated across two timesteps in that case.

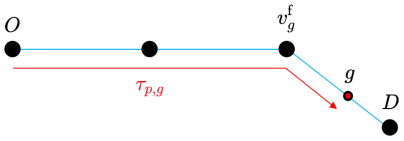

(a) Network representation of travel time from the origin O to a point g.

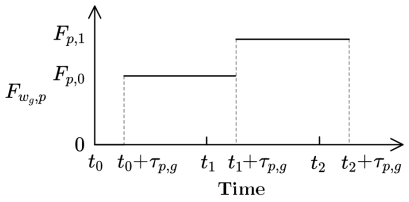

(b) The real-time path flow through point g given the path flow for two time periods $F_{p,0}$ and $F_{p,1}$ when the travel time $\tau_{p,g}$ is less than the duration of time interval T_{d}.

Figure 2: Illustration of the travel time and the real-time path flow at point g on a path p connecting OD pair w in an example network.

The accumulative path flows on a point g except for nodes in a k-th time interval can be derived as:

$$\hat{F}_{g,k} = \sum_{w \in \mathcal{W}} \sum_{p \in \mathcal{P}_w} F_{g,p,k}\delta_{e_g,p}, \quad g \in G \setminus \mathcal{V}, k = 1, \ldots, K \tag{11}$$

The flow on a link e in time interval k can then be defined with two parts: the inflow $f_{e,k}^{\mathrm{in}}$ and the outflow $f_{e,k}^{\mathrm{out}}$, where $f_{e,k}^{\mathrm{in}}$ is the total flow of N_s grid points on link e that is closest to the start point e_{s}:

$$f_{e,k}^{\mathrm{in}} = \sum_{g \in \boldsymbol{g}_{\mathrm{s}}} \hat{F}_{g,k}, \quad \boldsymbol{g}_{\mathrm{s}} = \underset{\boldsymbol{g}'_{\mathrm{s}} \subset \boldsymbol{g}_e, |\boldsymbol{g}'_{\mathrm{s}}| = N_s}{\arg\min} \sum_{g \in \boldsymbol{g}'_{\mathrm{s}}} d(g, e_{\mathrm{s}}), e \in \mathcal{E}, k = 1, \ldots, K \tag{12}$$

and $f_{e,k}^{\text{out}}$ is the total flow through the N_s grid points on link e that is closest to the end node e_{d}:

$$f_{e,k}^{\text{out}} = \sum_{g \in \boldsymbol{g}_{\text{d}}} \hat{F}_{g,k}, \quad \boldsymbol{g}_{\text{d}} = \underset{\boldsymbol{g}'_{\text{d}} \subset \boldsymbol{g}_e, |\boldsymbol{g}'_{\text{d}}| = N_s}{\arg\min} \sum_{g \in \boldsymbol{g}'_{\text{d}}} d(g, e_{\text{d}}), e \in \mathcal{E}, k = 1, \ldots, K \tag{13}$$

with $d(a, b)$ the Euclidean distance between point a and b.

Due to the limited traffic flow capacity f_e^{c} for each link, the link inflow and outflow are constrained so that the average flow speed $s_{e,k}$ can be specified as a reasonable value independent of the traffic density:

$$f_{e,k}^{\text{in}} \leq f_e^{\text{c}}, \quad e \in \mathcal{E}, k = 1, \ldots, K \tag{14}$$

$$f_{e,k}^{\text{out}} \leq f_e^{\text{c}}, \quad e \in \mathcal{E}, k = 1, \ldots, K \tag{15}$$

where f_e^{c} is the traffic flow capacity for link e.

2.3.2. Objectives

Firstly, we introduce the congestion cost $\mathscr{G}_{e,k}$ for each link e in time interval k. In addition to evaluating the traffic density of incoming and outgoing flow, the energy consumption of the air traffic flow on each link is taken into account. $\mathscr{G}_{e,k}$ is defined as follows:

$$\mathscr{G}_{e,k} = \sum_{R \in \{\text{in,out}\}} a\alpha_e f_{e,k}^R + b {f_{e,k}^R}^2, \quad e \in \mathcal{E}, k = 1, \cdots, K \tag{16}$$

where a, b are coefficients, and α_e is the energy consumption factor of link e defined to model the UAM operational efficiency according to the characteristics of links:

$$\alpha_e = \begin{cases} L_e \varphi_h, e \in \mathcal{E}_h \\ L_e \varphi_u, e \in \mathcal{E}_u \\ L_e \varphi_d, e \in \mathcal{E}_d \end{cases} \tag{17}$$

with φ_h, φ_u, and φ_d the efficiency coefficient per distance unit for horizontal $\mathcal{E}_h$, upward $\mathcal{E}_u$ and downward links $\mathcal{E}_d$, respectively.

The linear and quadratic form of link flow represents respectively the energy of displacement and the energy to maintain the free flow speed. The purpose of coefficients a and b is to pre-weight these terms. A feasible selection of these coefficients in the literature is $a = 1/|\bar{\alpha}\bar{f}_k|$, $b = 1/(4\bar{f}_k^2)$ (Delahaye, 1995), where $\bar{\alpha} = \sum_{e \in \mathcal{E}} \alpha_e / |\mathcal{E}|$, $\bar{f}_k$ is the average flow of all links in time interval k:

$$\bar{f}_k = \frac{\sum\limits_{e \in \mathcal{E}} f_{e,k}^{\text{in}} + f_{e,k}^{\text{out}}}{2|\mathcal{E}|} \tag{18}$$

Although the formulation of congestion cost is inspired by traditional ATM studies (Delahaye, 1995), the selection of coefficients does not rely on dimensional quantities but rather on relative weights assigned to flow and different energy consumption factors, which enables the extension of the formulation of congestion cost to the context of UTM. However, as mentioned previously, the congestion only reveals partial information about the complexity of UAM traffic. For example, Figure 5 gives four traffic scenarios with the same traffic density, but with very different complexity in managing the traffic. To access the interdependency between congestion and the difficulty of managing air traffic, the objective function takes into account the air traffic complexity cost and congestion cost.

In 3D UAM route networks, the air traffic complexity mainly occurs at intersections. The interactions between the different amounts of path flow from different directions can be complicated. Before modeling the complexity cost, we first define cylindrical airspace $\mathcal{A}_v$ around each node v. One way to determine the size of $\mathcal{A}_v$ is to include the first N_{r} rows of the grid closest to node v in the horizontal and vertical direction.

The density points involved in the cylinder are the observations to measure the air traffic complexity. Figure 3 provides an example of the cylindrical airspace around a node, which is connected by several one-way or two-way links. The density points involved in the cylinder are used to measure the air traffic complexity around the node.

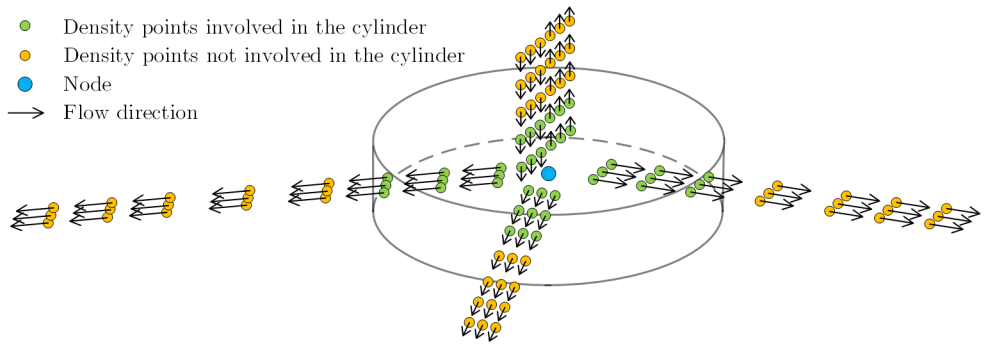

Figure 3: Example of cylindrical airspace around a node to measure the complexity of air traffic

The Linear Dynamical System (LDS) provides a strong theoretical framework for evaluating the intrinsic air traffic complexity by measuring the local disorder and interaction of UAM vehicles in a given zone of airspace. By representing the behavior of the system using a set of linear equations, the LDS model can effectively capture and quantify the level of disorder and interaction among a large number of aircraft, independent of airspace structure and ATC system. In addition, LDS contributes to improving situational awareness by providing a predictive framework that assists in anticipating and understanding the future behavior of UAM vehicles within specified airspace (Delahaye et al., 2022).

In three-dimensional Euclidean space, the LDS has the following form:

$$\dot{\mathbf{x}} = \mathbf{A}\mathbf{x} + \mathbf{b} \tag{19}$$

with $\mathbf{x}$ the state vector, $\dot{\mathbf{x}}$ the speed vector. $\mathbf{A} \in \mathbb{R}^{3\times3}$ a coefficient matrix, and $\mathbf{b} \in \mathbb{R}^3$ a coefficient vector.

To fit the observations of the aircraft in each cylindrical airspace $\mathcal{A}_v$ around node v at time interval k with LDS, we propose a Weighted Minimum Mean square Error (WMMSE) criterion. Traffic density $\rho_{g,k}$ is added in this formulation to indicate the importance of traffic flow on each grid g to the LDS over the time interval k. The WMMSE is given by:

$$\min_{\mathbf{A},\mathbf{b}} \sum_{g\in\mathcal{A}_v} \rho_{g,k} \|\dot{\mathbf{x}}_{g,k} - (\mathbf{A}\mathbf{x}_g + \mathbf{b})\|^2 \tag{20}$$

where $\mathbf{x}_g = (x_g, y_g, z_g)^\top$ is the position vector of point g. The speed vector of a point g depends on the type of associated link e_g:

$$\dot{\mathbf{x}}_{g,k} = \begin{cases} s_{g,k}(\cos(\theta_g), \sin(\theta_g), 0)^\top, & e_g \in \mathcal{E}_h \\ (0, 0, s_{g,k})^\top, & e_g \in \mathcal{E}_u \\ (0, 0, -s_{g,k})^\top, & e_g \in \mathcal{E}_d \end{cases} \tag{21}$$

where $s_{g,k}$ is the average flow speed on e_g in time interval k, and θ_g is the heading of flow.

The coefficient matrix $\hat{\mathbf{A}}$ and coefficient vector $\hat{\mathbf{b}}$ that minimizes the WMMSE can be calculated by Singular Value Decomposition (SVD). The calculation details of minimizing the WMMSE is outlined in Appendix A. Wang et al. (2022b) provided a proof that enables us to partially characterize the qualitative behavior in terms of the evolution of the LDS by examining the eigenvalues $\boldsymbol{\lambda} = \{\lambda_1, \lambda_2, \lambda_3\} \in \mathbb{C}^3$ of the coefficient matrix $\hat{\mathbf{A}}$. In this study, these eigenvalues indicate the complexity of the air traffic involved in the LDS. More specifically, the real part of each eigenvalue determines the stability of a particular component of the system state (Sayama, 2015). The positive real part of an eigenvalue is associated with the expansion mode and introduces divergence. The negative real part is associated with the contraction mode and

introduces convergence. Furthermore, the larger the absolute value of the real part of $\boldsymbol{\lambda}$, the faster the LDS evolves. In terms of the imaginary part of $\boldsymbol{\lambda}$, it has no impact on the stability of LDS as it determines the rotation tendency of the system. Those dynamics of LDS related to $\boldsymbol{\lambda}$ can be described in the complex plane in Figure 4.

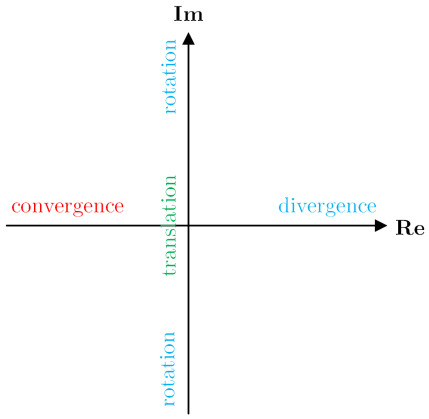

Figure 4: Evolution properties of the LDS in relation to eigenvalues of associated coefficient matrix $\mathbf{A}$

To bring theory closer to practice, four typical 3D traffic situations (translation, rotation, convergence, and divergence) and the eigenvalue loci of $\boldsymbol{\lambda}$ associated with each situation have been presented in Figure 5. The translation and rotation cases are two typical organized traffic situations with no potential conflict at that moment, as the distance between trajectory points remains constant. As we can see in Figure 5a and 5b, the real part of all eigenvalues is zero. In the convergence case, according to Figure 5c, the relative distances between trajectory points decrease with time. The eigenvalues are real negative, indicating that the LDS evolves in a contraction mode. A high level of air traffic complexity occurs as the trajectory points are converging. In the divergence case, according to Figure 5d, the real part of eigenvalues is positive, which corresponds to an expansion mode. The trajectory points are diverging and their relative distances increase with time, which avoids potential conflicts.

In sum, the translation, rotation, and divergence cases are linked to organized traffic situations, while the convergent case indicates unorganized traffic. Therefore, the eigenvalues with a negative real part represent disorderly traffic, and larger the absolute value represents more complex traffic conditions. Furthermore, it is important to note that most real-world traffic situations are often a combination of these typical scenarios. By blending different proportions of translation, rotation, convergence, and divergence, it becomes possible to represent and analyze a wide range of complex traffic dynamics that occur in practical air traffic scenarios. This flexibility in combining typical situations allows the associated LDS for providing a quantitative framework to study the mixed traffic situations and the intricate nature of real-world air traffic complexity.

We then define the complexity cost $\mathscr{X}_{v,k}$ for each node v over a time period k as the sum of the absolute value of negative real parts of $\boldsymbol{\lambda}$ of the LDS in the cylindrical airspace $\mathcal{A}_v$:

$$\mathscr{X}_{v,k} = \sum_{i=1}^{3} |\min(\mathrm{Re}(\lambda_i), 0)| \tag{22}$$

In order to better understand how the LDS-based air traffic complexity metric relates to air traffic assignment, we will provide an example for further explanation. It involves two most common scenarios in structured airspace: a merging case, where two flight paths converge and then continue as a single flow, and a crossing case, where two flight paths intersect without merging.

These two scenarios are visualized in Figure 6 within the context of SATA. In each scenario, upstream links have 100 link flows. Density points that are adjacent to each other are set 1km apart, and the average

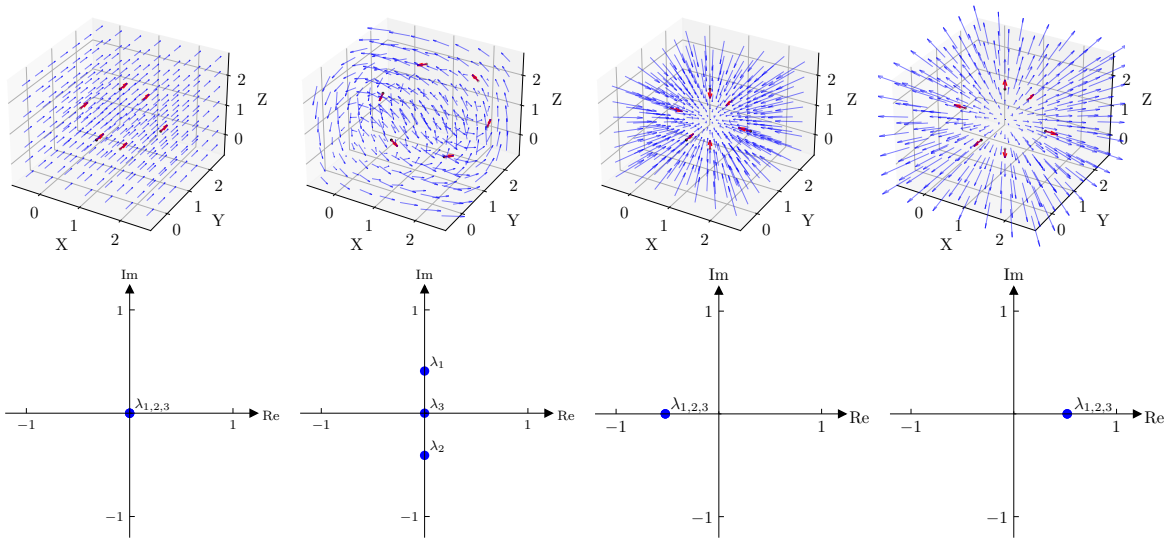

(a) Translation (b) Rotation (c) Convergence (d) Divergence

Figure 5: Eigenvalue loci for four typical traffic situations in three-dimensional airspace. The black dots represent the observed trajectory points of aircraft, the red arrows indicate their speed vectors, and the blue arrows indicate the speed vectors estimated by the LDS at equidistantly-partitioned points.

flow speed is 10 m/s. In the merging scenario, the traffic complexity calculated by equation (22) is notably high, approximately 6. Conversely, the crossing scenario has negligible complexity, approximating zero.

In a merging scenario, as the two traffic flows come together, they need to merge into a single flow. This requires careful speed and altitude adjustments to maintain safe separation between all aircraft, thereby increasing the associated air traffic complexity. In contrast, in a crossing scenario, while there is a point of intersection, aircraft are typically separated vertically to maintain safety. This simplifies the control task compared to the merging scenario, leading to a lower air traffic complexity. It's also worth noting that in our case, the crossing traffic flow is symmetric, which can potentially lead to a complexity metric of zero. This results from the fact that symmetric flows essentially balance each other out and no additional control efforts are needed for deconfliction.

These observations also align with simulation results from the Bluesky simulator, which indicate that the crossing case has a higher capacity compared to the merging case, and also exhibits more effective tactical deconfliction (Chen et al., 2022, 2023).

Finally, the objective function $\mathscr{C}$ is defined as the weighted sum of the air traffic complexity and congestion of UAM operations:

$$\mathscr{C} = (1-\phi)\sum_{k=1}^{K}\sum_{v\in\mathcal{V}}\mathscr{X}_{v,k} + \phi\sum_{k=1}^{K}\sum_{e\in\mathcal{E}}\mathscr{G}_{e,k} \tag{23}$$

where $\phi \in [0,1]$ is the weighting parameter to control the cost of each group. Since these two costs measure the disorder of air traffic from different perspectives, they can be seen as independent of each other. The parameter ϕ should be selected to balance the magnitude of the total complexity cost and congestion cost to make them equally important.

3. Optimization algorithm for the QATA problem

3.1. Simulation-based rolling horizon framework

Conventional traffic assignment algorithms assume the cost function to be convex and separable with respect to link flow, which is not always true in real operations. For example, in some complex traffic

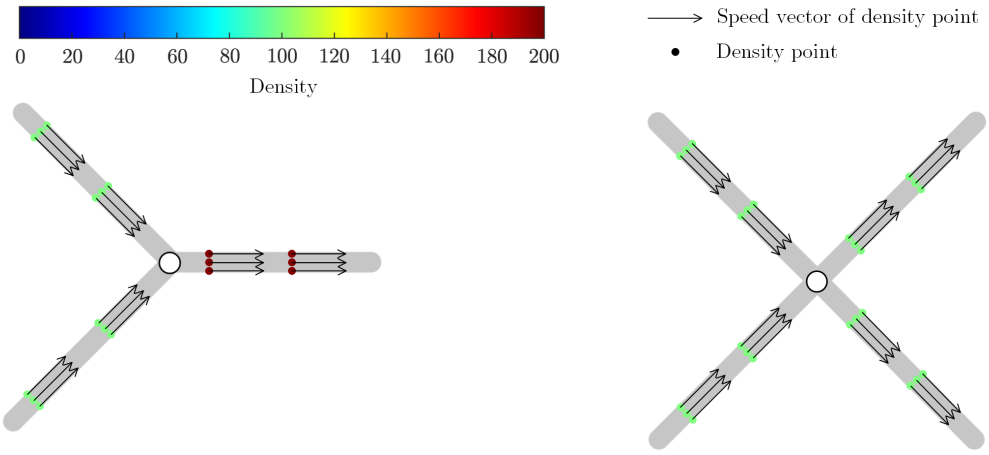

(a) Merging (b) Crossing

Figure 6: A toy example of integrating the LDS into air traffic assignment

situations such as the intersection of several links with dense traffic flow, the cost function can be modeled to evaluate the air traffic complexity in a non-separable way, such as equation (22). In addition, the cost function may be also non-convex in some cases, even without analytical form.

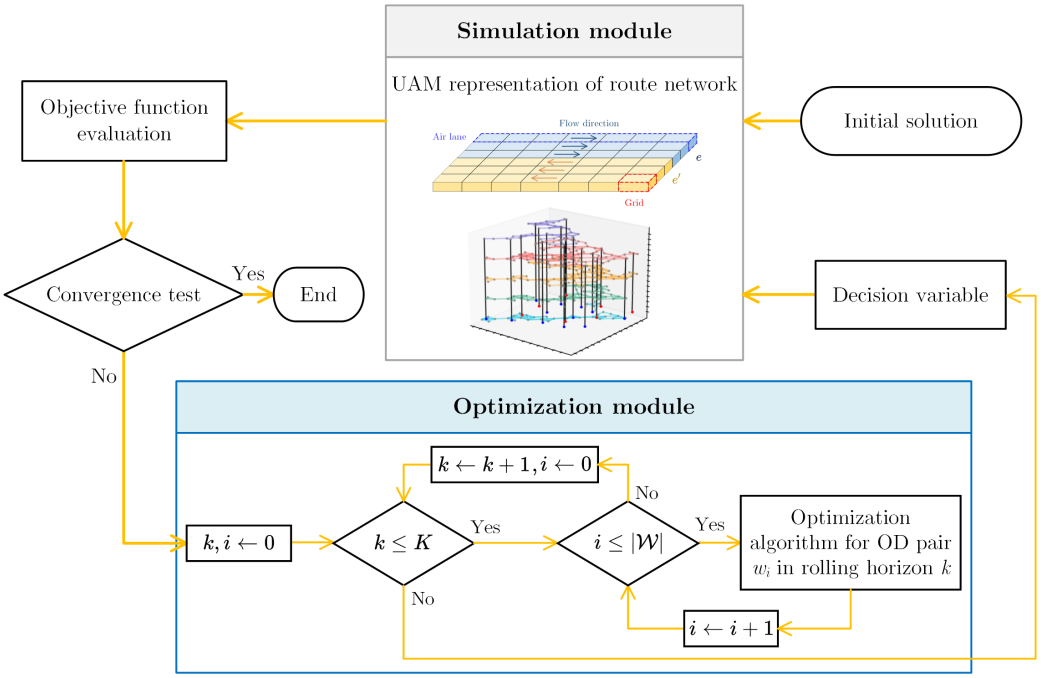

Figure 7: Flowchart of a simulation-based framework for solving the QATA optimization problem. The simulation module includes the UAM representation of the route network, and the optimization module contains the optimization algorithm in a nested loop over OD pairs and rolling horizons.

As a consequence, a simulation-based framework is proposed to solve the QATA problem. The associated flowchart is shown in Figure 7. The framework begins with an initial path flow pattern. To provide high-quality initial flow patterns to improve the efficiency of the simulation module, we investigate a randomized

approach based on the All-Or-Nothing (AON) assignment to initialize flow patterns with relatively low objective values. For each OD pair w and time interval k, firstly, a path flow pattern is randomly generated. Then, based on the current path flows, we define the path cost in the following form:

$$\mathscr{C}_{p,k} = (1-\phi)\sum_{v\in p}\mathscr{X}_{v,k} + \phi\sum_{e\in p}\mathscr{G}_{e,k}, \quad p\in\mathcal{P}_w, w\in\mathcal{W}, k=1,\cdots,K \tag{24}$$

Then, the AON assignment is performed on paths in $\mathcal{P}_w$:

$$\gamma_{p,k} = \begin{cases} 1, & p = \arg\min_{p\in\mathcal{P}_w}\mathscr{C}_{p,k} \\ 0, & \text{otherwise} \end{cases} \tag{25}$$

This initialization strategy is adapted to the objective function. It is able to provide an initial path flow pattern with relatively low air traffic complexity and congestion, which will improve the efficiency of the optimization algorithm.

Two main modules are contained in this framework: the simulation module and the optimization module. The simulation module includes the modeling of a 3D route network under UAM representation. Together with the network dynamics, it supports calculating the characteristics of the route network and the objective function $\mathscr{C}$. In the optimization module, a rolling horizon approach is introduced to address the QATA problem in the planning horizon by decomposing the original problem into several sub-problems. This approach results in substantial savings in computational time while preserving the relationship between the different time intervals. Each sub-problem k can be formulated as a modified SATA problem, with the objective function as

$$\mathscr{C}_k = (1-\phi)\sum_{v\in\mathcal{V}}\mathscr{X}_{v,k} + \phi\sum_{e\in\mathcal{E}}\mathscr{G}_{e,k}, \quad k=1,\ldots,K \tag{26}$$

and constraints defined by equations (4)-(15).

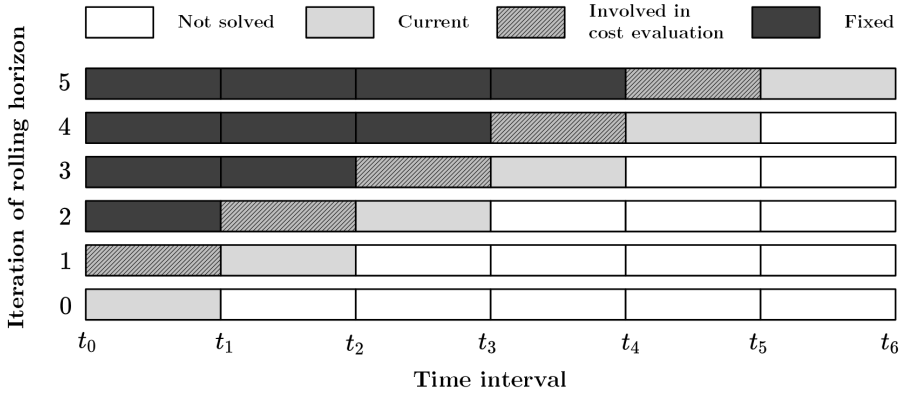

Figure 8: General strategy of the optimization module to approximate the optimal flow pattern of QATA using rolling horizon approach. This example includes six time intervals and the maximum time gap is less than the duration of the time interval. Inner loops are conducted for each OD pair in each time interval.

In order to evaluate $\mathscr{C}_k$, previous time intervals $\{k-1,\cdots,k-N_{\max}\}$ should be considered, where $N_{\max} = \lceil \max_{g\in p, p\in P_w, w\in W}\tau_{p,g}/T_{\mathrm{d}}\rceil$. Indeed, due to the residual demand, except for the first time interval, the flow pattern in each time interval is determined based on the results of $N_{\max}$ previous time intervals. Figure 8 gives the scheme of the rolling horizon, corresponding to the case in which the maximum time gap is less than the time interval T_{d}, that is, $N_{\max}=1$. In this study, the time length of each rolling horizon and the time shift are both set to T_{d}. The start time and the end time of each rolling horizon are aligned with each time interval. Sliding along the time axis, the rolling horizon begins at t_0, and the optimization algorithm is applied in the time interval $[t_0,t_1]$. Next, the rolling horizon is shifted by T_{d}, and the current

interval for optimization becomes $[t_1, t_2]$. The receding process is repeated until the final rolling horizon $[t_{K-1}, t_K]$ is reached. Since the maximum time gap in this example is less than the duration of the time interval, in Figure 8, only the current and last time intervals are involved to calculate $\mathscr{C}_k$ in time intervals $k = 1, \cdots, 5$. The path flow is updated in each OD according to the cost function or performance indicators.

The optimization module, as shown in Figure 7, directly controls and updates the decision variables γ in a nested loop over OD pairs and sub-problems. This formulation strengthens the connection between sub-problems by collaboratively adjusting the decision variables involved in each rolling horizon. A simulated annealing algorithm using parallel computing and a novel neighborhood generation strategy is proposed as the optimization algorithm in the optimization module, which will be introduced in the next section. Thus, based on the current decision variables, the simulation module generates the flow pattern for calculating the value of objective function $\mathscr{C}$, which guides the optimization module to approximate the optimal QATA solution with low air traffic congestion and complexity. Finally, each outer loop performs a convergence test. If the stopping criterion is reached, the whole framework will be terminated.

The main advantages of this framework can be listed as follows:

- The route network has been already designed in the previous study. A feasible path set is created in advance for each OD. Each feasible path set includes K-shortest paths that minimize operational cost, efficiency cost, and safety cost of the route network. This avoids the heavy computation of searching shortest paths and extra cost function evaluation for large-scale route networks.

- The rolling horizon approach in the optimization module can reduce the problem size and computational burden of cost function evaluation. The decision variables involved in each rolling horizon are collaboratively updated to strengthen the connection between sub-problems. Moreover, it also enables a refined optimization with fewer uncertainties in the search space.

- Other than most traffic assignment algorithms based on several simulation environments, only one simulation environment will be created for each individual process, which improves the calculation efficiency.

3.2. Parallel simulated annealing algorithm

As the QATA is an optimization problem with continuous variables and a non-differentiable objective, from the operational point of view, a near-optimal solution is required, rather than a globally optimal solution, which exists theoretically but is difficult to achieve in the limited computational time. The metaheuristic algorithms are very suitable for such problems. They are capable of handling NP-hard problems with high-dimensional state spaces. The SA is a commonly used non-population-based metaheuristic optimization algorithm. Analogous to physical annealing in metallurgy, it has the stochastic convergence property (Kirkpatrick et al., 1983). In this study, we redesign the classical SA algorithm and introduce a PSA algorithm with a novel neighborhood generation strategy and parallelized cost function evaluations to efficiently optimize the simulation-based QATA problem.

The asymptotic convergence of the SA to the global optimum is highly dependent on the selection of neighborhood (Fleischer and Jacobson, 1999). For the QATA problem, we propose a novel strategy to generate the neighborhood solution. The pseudocode is presented in Algorithm 1. To generate the neighboring solution that moves effectively and efficiently, we focus on transferring the flow from one path to another in each OD pair in each transition. The outflow and inflow paths are chosen randomly, whereas the outflow path is chosen only from the paths with the non-zero flow. To avoid redundant operations on paths with less traffic, we determine the transferring flow σ by comparing the flow of outflow path $\gamma_{p_i,k}$ with the threshold $F_t/D_{w,k}$ (line 6). If $\gamma_{p_i,k}$ is larger, the flow to be transferred will be drawn from a uniform distribution between zero and $\gamma_{p_i,k}$. Otherwise, the outflow path will transfer all its flow. In this way, only constraints (14) and (15) are required to be ensured, and all other constraints are satisfied.

Given a neighboring solution, we need to update the objective function to determine whether to accept this solution. Due to the separability of the objective function (26) of rolling horizons, it is noteworthy that the objective function may be updated through the simulation module without involving all decision variables, by calculating the incremental difference of the objective function value. To further speed up the

optimization algorithm, the objective function is evaluated in parallel. Unlike problem-independent parallelization methods that involve frequent evaluations of the objective function (Onbaşoğlu and Özdamar, 2001), we design a problem-dependent parallelization approach by dividing $\Delta C_{w,k}$ among multiple threads. As the evaluation of the objective function is computationally expensive, especially in solving the WMMSE and computing the eigenvalues, the objective function is only calculated if necessary and updated incrementally. The pseudocode of this parallel computing strategy is formulated in Algorithm 2. After completely computing the objective function (23), for each OD pair w and rolling horizon k, we first generate the neighboring solution and submit the evaluation of associated complexity costs to the task queue (lines 2-4). The task queue is executed concurrently by multiple threads and placed in a completed task queue (lines 5-7). A thread pool is used in this process to avoid latency. The congestion costs are not involved in parallel computing as they are straightforward to compute. The change in the objective function value of neighboring solutions is computed based on the completed task queue (lines 8). The Metropolis criterion is used as the acceptance criterion (Metropolis et al., 1953). If the generated neighboring solution is accepted, the current solution and costs will be updated in terms of the impacted paths (lines 9-13).

Also note that, after the cost evaluation and update for each time interval, the complexity cost for the next time interval is required to be completely computed to update with the modifications of the flow pattern in the last time interval.

Algorithm 1 Neighborhood generation method for QATA problem

1: **procedure** NEIGHBORHOODGENERATION($\boldsymbol{\gamma}_{w,k}$)
2: **do**
3: $\hat{\boldsymbol{\gamma}}_{w,k} \leftarrow \boldsymbol{\gamma}_{w,k}$
4: $p_1 \leftarrow$ path randomly selected from $\mathcal{P}$ with non-zero flow
5: $p_2 \leftarrow$ path randomly selected from $\mathcal{P}_w$ different from p_1
6: $\sigma \leftarrow \begin{cases} \text{UNIFORM}(0, \gamma_{p_1,k}), \gamma_{p_1,k} \geq \frac{F_t}{D_{w,k}} \\ \gamma_{p_1,k} \qquad\qquad\qquad , \gamma_{p_1,k} < \frac{F_t}{D_{w,k}} \end{cases}$
7: $\hat{\gamma}_{p_1,k} \leftarrow \gamma_{p_1,k} - \sigma$
8: $\hat{\gamma}_{p_2,k} \leftarrow \gamma_{p_2,k} + \sigma$
9: **while** (Constraint (15) is not satisfied)
10: **return** $\{p_1, p_2\}$, $\hat{\boldsymbol{\gamma}}_{w,k}$
11: **end procedure**

PSA is stopped if any of the following stopping criteria are met:

1. $(\hat{\mathscr{C}} - \hat{\mathscr{C}}_c)/\hat{\mathscr{C}} < 0.1\%$, if the best objective value $\hat{\mathscr{C}}_c$ of current temperature is improved less than 0.1% than previous one $\hat{\mathscr{C}}_c$;
2. $T_c < 10^{-4} T_{\text{init}}$, if the current temperature is less than 10^{-4} of initial temperature.

4. Experiments

We develop a parcel delivery scenario involving intensive UAM operations within a centralized control scheme, specifically implemented in Singapore's urban airspace. The associated UAM route network is shown in Figure 9b. It was designed by Wang et al. (2022a) to maximize network efficiency and flight safety and to minimize noise impact on the population. There are a total of 7 vertiports and 12 delivery sites distributed throughout the city, resulting in a total of 84 OD pairs. This UAM network consists of five horizontal layers connected by a limited number of vertical links. The connections and geographical locations of these vertiports and delivery sites are visualized in Figure 9a. The candidate paths between each OD pair are selected using the K-shortest path search algorithm with diversity (Liu et al., 2017). Some basic topology features of the UAM route network are summarized in Table 2 for each layer and the network in order to offer insights into the network's connectivity, clustering patterns, and assortative mixing behavior. These features include the number of nodes, the number of links, Average Degree (AD), Average Clustering

Algorithm 2 Incremental parallel cost calculation and update

procedure CostEvaluation($\boldsymbol{\gamma}_{w,k}$, $\boldsymbol{X}$, $\boldsymbol{G}$)
  $TQ \leftarrow \emptyset$ ▷ Task queue
  $\hat{\boldsymbol{p}}, \hat{\boldsymbol{\gamma}}_{w,k} \leftarrow$ NeighborhoodGeneration($\boldsymbol{\gamma}_{w,k}$)
  $TQ \leftarrow \bigcup_{v \in \hat{\boldsymbol{p}}} \mathscr{X}_{v,k}(\hat{\boldsymbol{\gamma}}_{w,k})$
  do
    $TQ_{\text{comp}} \leftarrow$ Invoke(TQ) ▷ Concurrent execution by multiple threads of tasks submitted to TQ, until all tasks have been completed
  while ($TQ \neq \emptyset$)
  $\Delta C_{w,k} \leftarrow (1-\phi) \sum_{v \in \hat{\boldsymbol{p}}} (X_{v,k} - \mathscr{X}_{v,k}(\hat{\boldsymbol{\gamma}}_{w,k})) + \phi \sum_{e \in \hat{\boldsymbol{p}}} (G_{e,k} - \mathscr{G}_{e,k}(\hat{\boldsymbol{\gamma}}_{w,k}))$
  if Accept($\Delta C_{w,k}$) **then**
    $\boldsymbol{\gamma}_{w,k} \leftarrow \hat{\boldsymbol{\gamma}}_{w,k}$
    $X_{v,k} \leftarrow \mathscr{X}_{v,k}(\boldsymbol{\gamma}_{w,k}),\ v \in \hat{\boldsymbol{p}}$
    $G_{e,k} \leftarrow \mathscr{G}_{e,k}(\boldsymbol{\gamma}_{w,k}),\ e \in \hat{\boldsymbol{p}}$
  end if
  return $\boldsymbol{X}$, $\boldsymbol{G}$, $\boldsymbol{\gamma}_{w,k}$
end procedure

Coefficient (ACC) (Saramäki et al., 2007), and Degree Of Assortativity (DOA) (Newman, 2003). According to hourly demands given in advance, a certain type of UAVs make deliveries from vertiports to delivery sites in this UAM route network. However, due to the presence of dense obstructions at low altitudes, the UAM route network offers limited route options, posing significant challenges in optimally assigning the UAM traffic flow. We summarize the parameter settings of the proposed simulation-based framework in Table 3.

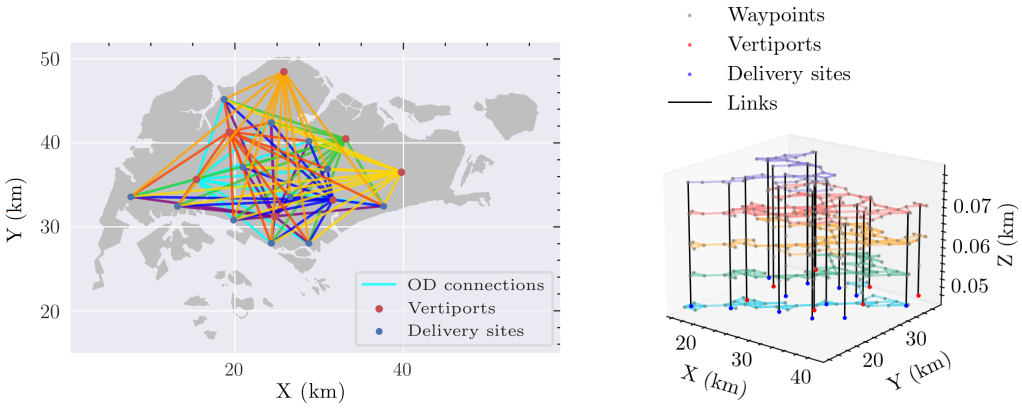

(a) Connection of OD pairs between delivery sites and vertiports.

(b) Network representation.

Figure 9: 3D UAM route network in Singapore's urban airspace.

The time-varying traffic demands (Figure 10) are focused on six peak hours of the day, from 09:00-10:00 to 14:00-15:00. For future high-density UAM operations, these demands are simulated based on the expected hourly number of parcel delivery UAVs in metropolitan areas predicted by Doole et al. (2020) and the distribution of hourly demand between several ODs for an urban network during a day (Deng et al., 2019).

To evaluate the effectiveness and performance of the proposed PSA, we also conduct a comparison study with representative conventional DTA algorithms for this QATA problem. Ameli et al. (2020b) made a cross-comparison between optimization algorithms for DTA and suggested that most conventional DTA

Table 2: Basic topology features of different altitude layers and the UAM route network.

Network	Number of nodes	Number of links	AD	ACC	DOA
Network layer at 150ft	51	96	4.57	0.35	-0.19
Network layer at 175ft	62	145	5.27	0.41	-0.12
Network layer at 200ft	85	216	5.20	0.32	0.31
Network layer at 225ft	89	199	4.47	0.24	0.23
Network layer at 250ft	45	89	3.96	0.18	0.33
The whole route network	332	745	5.00	0.23	0.23

Table 3: parameters setting in the experiment.

Module	Parameter	Value	Description
Simulation module	L_h	0.15 (km)	Grid length of horizontal volume segment
	L_v	1e-3 (km)	Length of grid on vertical volume segments
	L_w	0.03 (km)	Grid width
	s_h	54 (km/h)	Speed for horizontal link e_h
	s_v	15 (km/h)	Speed for vertical link e_v
	N_s	3	Number of lateral points on each side
	N_{r}	3	Number of rows of the grid included by cylindrical airspace
	F_t	20 (veh/h)	Meaningful flow threshold e
	f_e^c	1.5e4 (veh/h)	Traffic flow capacity for link e
	φ_h	0.2	Efficiency coefficient for horizontal links
	φ_u	1	Efficiency coefficient for upward links
	φ_d	0.02	Efficiency coefficient for downward links
	ϕ	0.9	Weighting parameter in objective function
Optimization module	T_{init}	100	Initial temperature
	N_{tr}	100	Number of iterations at each temperature
	α	0.9	Cooling rate
	ε	0.01	Small variation for numerical derivation in DA

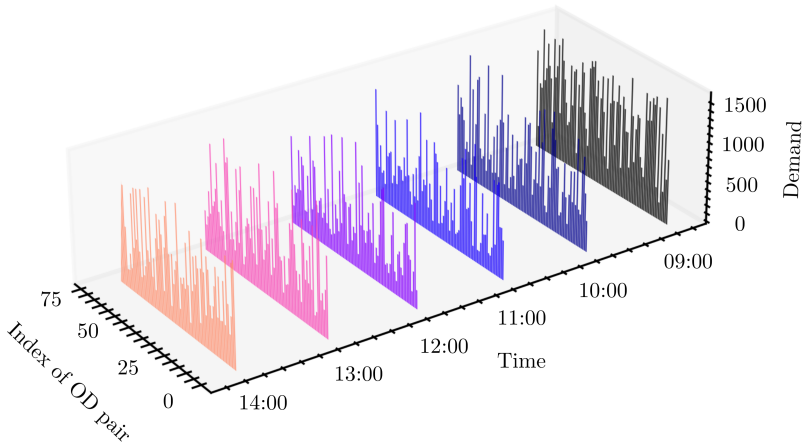

Figure 10: Simulated hourly UAM traffic demands for each OD pair from 09:00-10:00 to 13:00-14:00.

algorithms including the method of successive average (Robbins and Monro, 1951) and its extensions (Lu et al., 2009, Sbayti et al., 2007) only exhibit good performance in small-scale networks and classical DTA problem formulation. They also proposed a Probabilistic Method (PM) that has better performance in a medium or large-scale network. In addition, we also compare PSA with another commonly used traffic assignment algorithm, namely Dafermos' Algorithm (DA) (Dafermos and Sparrow, 1969, Dafermos, 1971, 1972), which has been used and performed well in our previous studies. These algorithms are also integrated into the simulation-based framework described in Figure 7. The details of these comparative algorithms can be referred to in Appendix B.1. The stopping criteria for these algorithms are in accordance with PSA. Note that, due to the limitations of traditional traffic assignment algorithms for this QATA problem in terms of network size, traffic volume, and mathematical formulation, we only select representative algorithms for comparison with our proposed algorithm to demonstrate the performance of PSA on UAM route networks with high-density traffic volume, high complexity, and congestion. All algorithms are implemented in Java on a laptop equipped with Intel®i7-12700H CPU and 16GB DDR5 RAM.

4.1. Performance analysis of PSA algorithm

4.1.1. Parallelization performance

To evaluate the computational time improvement of the proposed acceleration strategy in terms of SA, we conduct the experiment on this scenario by increasing the number of threads from 1 to 20. It is noteworthy that the single-thread case is similar to a sequential process. For each number of threads, we record 10,000 times the CPU time for a transition in different temperatures throughout the optimization process of SA.

Figure 11 shows the boxplots of the computational time of a transition in PSA for different numbers of threads. It can be noted that the performance is not significantly improved when more than 8 threads are used. The results indicate that the proposed parallel strategy can result in a speedup of nearly three times over the sequential approach by using a sufficient number of threads. The CPU time per transition of PSA using 20 threads can be reduced to $(9729 \pm 2.5) \times 10^{-5}$s in 95% confidence interval. It is quite efficient since each transition includes the cost evaluation and update for all OD pairs and all time intervals, which is $K|\mathcal{W}| = 504$ times in this studied case. Averaged over each operation, Algorithm 2 only takes less than 0.2ms.

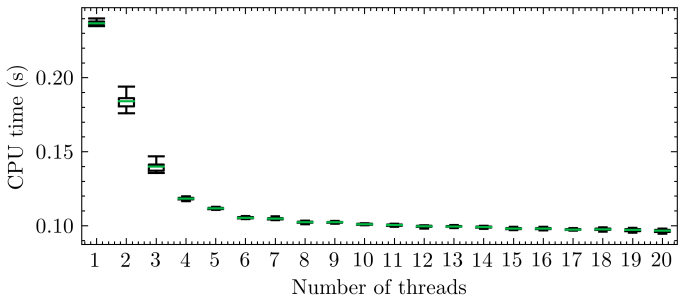

Figure 11: Run time for a transition in PSA with the different number of threads. The median is indicated in green. The lower bound and upper bound of the box represent respectively the first and third quartile. The whiskers above and below the box include the values between the 5th and 95th percentiles.

4.1.2. Comparison with conventional traffic assignment algorithms

In addition to the objective function, the flight efficiency in the UAM route network is also measured to ensure that it is at an acceptable level. Two indicators are introduced, including average travel time $\bar{t}$:

$$\bar{t} = \frac{\sum_{k=1}^{K} \sum_{w \in \mathcal{W}} D_{w,k} \sum_{p \in \mathcal{P}_w} \gamma_{p,k} \sum_{e \in p} L_e / s_e}{\sum_{k=1}^{K} \sum_{w \in \mathcal{W}} D_{w,k}} \tag{27}$$

and average path length $\bar{l}$:

$$\bar{l} = \frac{\sum_{k=1}^{K} \sum_{w \in \mathcal{W}} D_{w,k} \sum_{p \in \mathcal{P}_w} \gamma_{p,k} \sum_{e \in p} L_e}{\sum_{k=1}^{K} \sum_{w \in \mathcal{W}} D_{w,k}} \tag{28}$$

For all algorithms, We performed 100 experiments with different random seeds, where the random seeds control the initial values and the inherent randomness of the algorithm. Table 4 illustrates the experimental results of all aforementioned algorithms. 95% Confidence Interval (CI) for the standard normal distribution is used to report the results, and the format is the sample mean plus/minus margin of error. The best result in each column is underlined. In addition, Figure 12 visualizes the reduction of objective function values obtained by these algorithms. As the performance of DA and PM is close, we additionally compare the objective function values produced by these two algorithms.

Table 4: Performance comparison of PSA and representative conventional DTA algorithms in terms of computation time, objective function, and flight efficiency for a 95% CI.

Models	Computation time (s)	Value of objective function	Complexity cost	Congestion cost	Average travel time (s)	Average path length (km)
Initial	-	99081.42 ± 368.48	585380.95 ± 3627.11	45048.14 ± 27.92	1201.94 ± 0.41	17.84 ± 0.01
PSA	143.47 ± 3.74	$\underline{67157.45 \pm 146.87}$	$\underline{302743.55 \pm 1574.53}$	$\underline{40981.22 \pm 36.90}$	1233.61 ± 0.48	18.28 ± 0.01
PM	$\underline{12.315 \pm 4.30}$	95926.01 ± 122.50	557388.35 ± 1260.06	44652.42 ± 65.67	1231.31 ± 0.57	18.23 ± 0.01
DA	502.15 ± 6.68	94361.08 ± 236.84	541264.75 ± 2368.71	44705.12 ± 26.23	$\underline{1198.18 \pm 0.38}$	$\underline{17.78 \pm 0.01}$

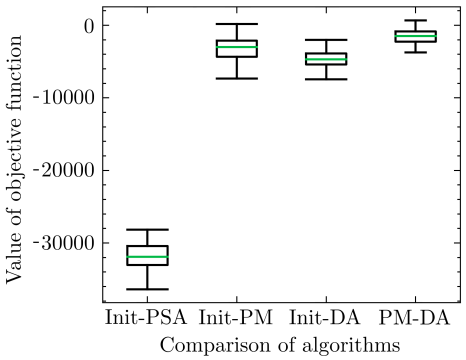

Figure 12: The reduction of objective function value after optimization of different algorithms compared to the initial state and the performance comparison between PM and DA. The boxplot is represented in the same way as Figure 11.

As for representative conventional DTA algorithms including DA and PM, there is no significant reduction in the value of objective function compared to PSA. This result may be explained by the fact that several assumptions for conventional DTA algorithms are not fully satisfied in the QATA formulation. In particular, the objective function does not have an analytical form and is not guaranteed to be convex, which may make traditional DTA algorithms easily fall into local optima. Another important point lies in the scale of the problem. With high-density traffic volume and large network size, traditional DTA algorithms may not be applicable to this scenario. In terms of the computation time, PM is much lower than other algorithms. DA takes the longest computation time, but the objective function value of DA is better than PM. DA also produces the flow pattern with the best flight efficiency.

In view of the proposed model PSA, the value of the objective function is significantly reduced by $(32.20 \pm 0.29)\%$. In the objective function, the complexity cost has been reduced by almost half. There is a limited reduction in congestion of nearly 10%. A possible reason could be the limited path selection

in the network and the low congestion level of the initial flow pattern. The computation time of PSA is also satisfying, considering the large size of the network, the high-density traffic volume, and the heavy computation involved in the LDS. The differences in average travel time and path length are quite small compared to the best results, which demonstrate that the flight efficiency of flow patterns obtained by PSA is not degraded. In summary, the proposed PSA algorithm is able to output the flow pattern with a significantly decreasing air traffic complexity and low congestion in a reasonable time, without degrading the flight efficiency, which supports the primary objective of this study.

To further analyze the optimization results at the operational level, the path flow allocation, link flow allocation, air traffic complexity, and congestion in the UAM route network will be presented in the following sections.

4.1.3. Path flow allocation

To initiate our analysis, we present the initial and PSA-optimized path flow allocations for comparison. The x-axis denotes the index of paths, while the y-axis corresponds to the index of time intervals, spanning from 09:00-10:00 to 14:00-15:00. Dashed white lines separate adjacent OD pairs. The color attributed to each path at each time interval represents the corresponding path flow.

the initial path flow allocations in each time interval are illustrated in Figure 13. Due to the high amount of paths in each OD pair, the initial path flow allocations are segmented into 4 subfigures. As can be observed in Figure 13, the demand is completely allocated to a specific path in each OD pair. Although the initial path flow pattern following the AON strategy has a low congestion level, there is still considerable potential to reduce air traffic complexity by better distributing traffic on various candidate paths. Additionally, in many OD pairs, the demand is assigned to the same path across all time intervals. The impact of the residual path flow in previous intervals on the current time interval requires the consideration of their interdependency. For each OD pair, it could be a preferable solution to have different flow allocation results for different time intervals.

The path flow distribution optimized by PSA is represented in Figure 14. A significant difference compared to Figure 13 can be observed in that the demands for each OD and time interval can be assigned to multiple paths. In addition, most OD pairs have different path flow patterns across time intervals. This fact demonstrates that after being optimized by PSA, the candidate paths can be sufficiently and optimally utilized to mitigate congestion and air traffic complexity. The optimization results can be accurately and clearly provided to ATC service providers and aircraft operators for implementation in the form of the number of flows on each path in each time interval.

4.1.4. Link flow allocation

Another important illustration lies in the link flow allocation. Figure 15 presents the initial link flow allocation in each time interval in the network representation. The color representation is logarithmic to cover a large range of link flow values. According to all subfigures, the traffic flow is mainly distributed on the three lower layers and the vertical links connecting them. The two upper layers are not fully used, especially the top layer. In accordance with the initial path flow distribution result in Figure 13 that the demand is assigned to the same path in many OD pairs across all time intervals, the link flow distribution is similar for different time intervals.

The link flow distribution optimized by PSA is shown in Figure 16. Compared with the initial link flow pattern in Figure 15, the link flows are distributed in all layers. It is also worth noting that, in network layers with few links and low connectivity such as the top layer and bottom layer, the links are assigned with relatively less flow. An explanation could be that UAM operations in these layers are more likely to introduce congestion and air traffic complexity. On the contrary, the link flows are densely concentrated in the middle layers and the vertical links connecting them. Since there are more route choices in these layers, a large number of link flows can be enabled to operate without bringing high congestion and air traffic complexity. Furthermore, given with time-varying demand for each time interval, the link flow patterns in these subfigures are slightly different, with regard to the amount of link flow and link usage.

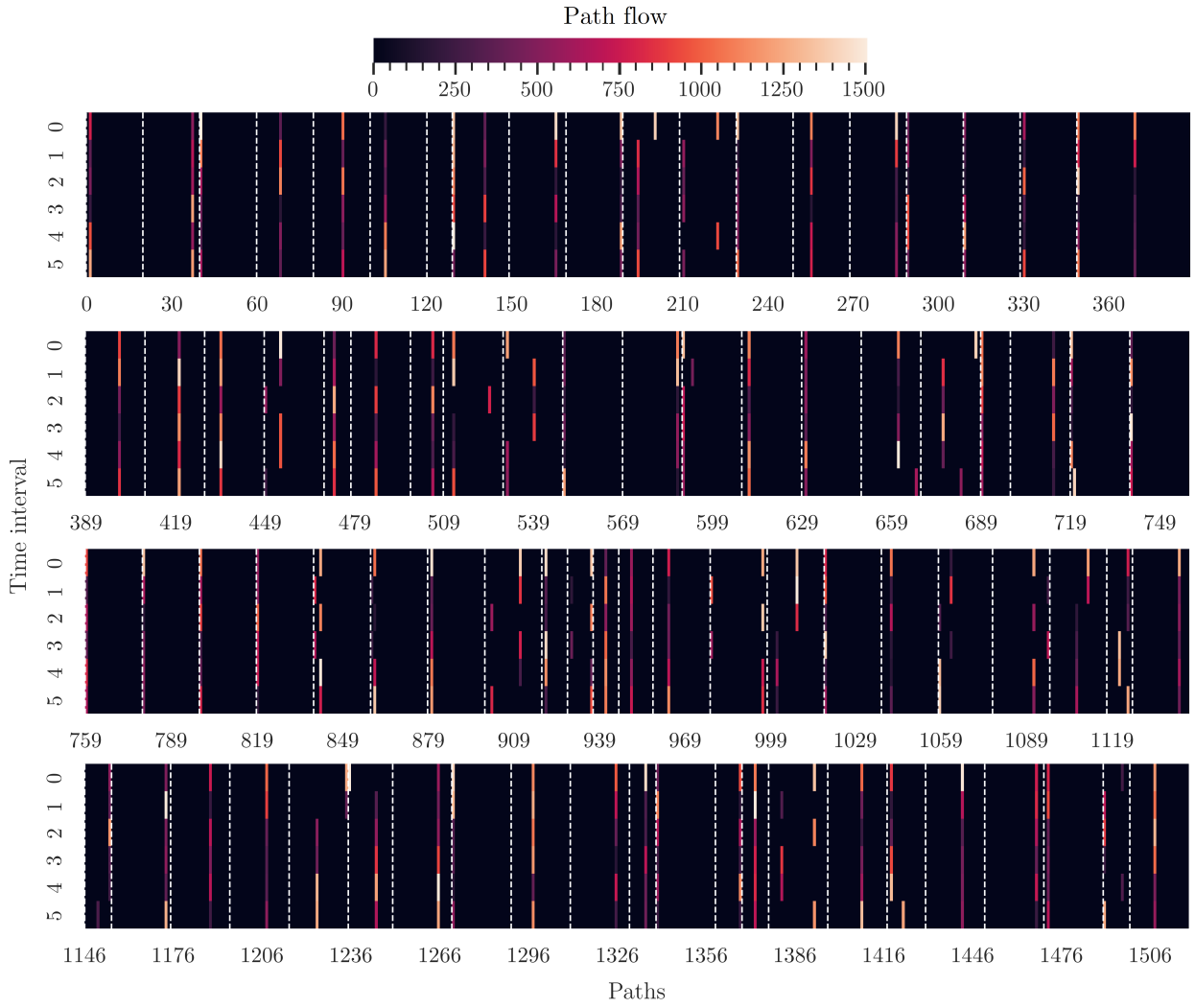

Figure 13: Initial path flows distribution in different time intervals.

4.1.5. Air traffic complexity and congestion

To evaluate the air traffic complexity and congestion, we illustrate the initial and optimized complexity cost and congestion cost in the network representation in Figure 17 and Figure 18, respectively. The color of each node represents the complexity cost, and the width of each link represents the congestion cost. As can be seen in Figure 17, the initial flow pattern involves high complexity costs. Each layer has a large number of nodes with a high level of complexity. The congestion mainly occurs in vertical links, especially the vertical links connecting the bottom three layers. This fact also demonstrates that initial flow patterns are mainly assigned in the lower layers. After optimization by PSA, it can be seen from Figure 18 that the complexity cost has been obviously reduced to a low level, especially for nodes in the three middle layers. Even for the top layer and bottom layer that have limited route choices, PSA is still capable of mitigating the air traffic complexity. The complexity cost of almost all nodes has been decreased to below 2000. With respect to the congestion cost, unlike Figure 17 in which the traffic congestion is mainly concentrated on vertical links, in Figure 18, a large part of congestion is distributed on horizontal links in each layer. Except for Figure 18(a), the congestion on vertical links is also reduced. The optimized flow pattern allows congestion to be spread throughout the network to reduce overall air traffic congestion.

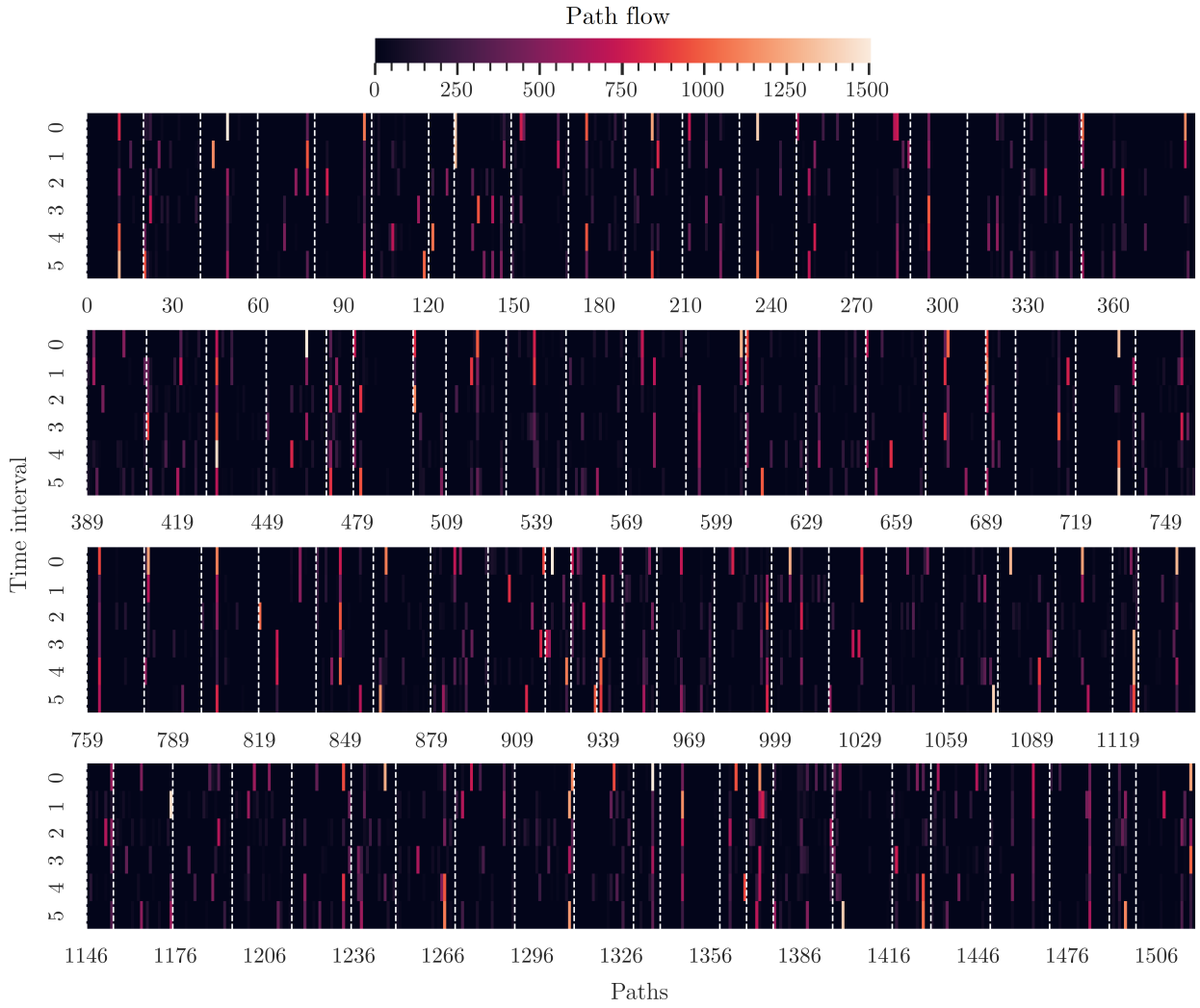

Figure 14: Distribution of path flows optimized by PSA in different time intervals.

We further explain the variations from the initial flow pattern to the optimized flow pattern in terms of complexity cost per node and congestion cost per link. This is visualized in Figure 19 and Figure 20, respectively. Each figure includes a colorbar, denoting the changes in cost values. Essentially, we aim to provide a clearer understanding of the extent of cost variation from Figure 17 to 18 from a global perspective rather than within the context of the UAM network representation. This allows us to capture and understand the network-wide effects of the QATA model and the implications of the cost variations.

Taking a closer look at Figure 19, the majority of changes were made to reduce the complexity associated with nodes across various time intervals. This is particularly evident for nodes initially characterized by high complexity, where a substantial decrease can be observed.

As depicted in Figure 20, a significant portion of air traffic congestion has been alleviated on numerous links across different time periods. However, it is important to note that despite the overall reduction, there are instances where congestion has increased on some links. This pattern is in accordance with the information presented in Figure 18. The strategy, instead of concentrating on the mitigation of congestion on specific links, seeks to optimally distribute congestion across the entire UAM route network. This optimally distributed congestion allows for more efficient use of the UAM network's capacity and a more effective UAM system.

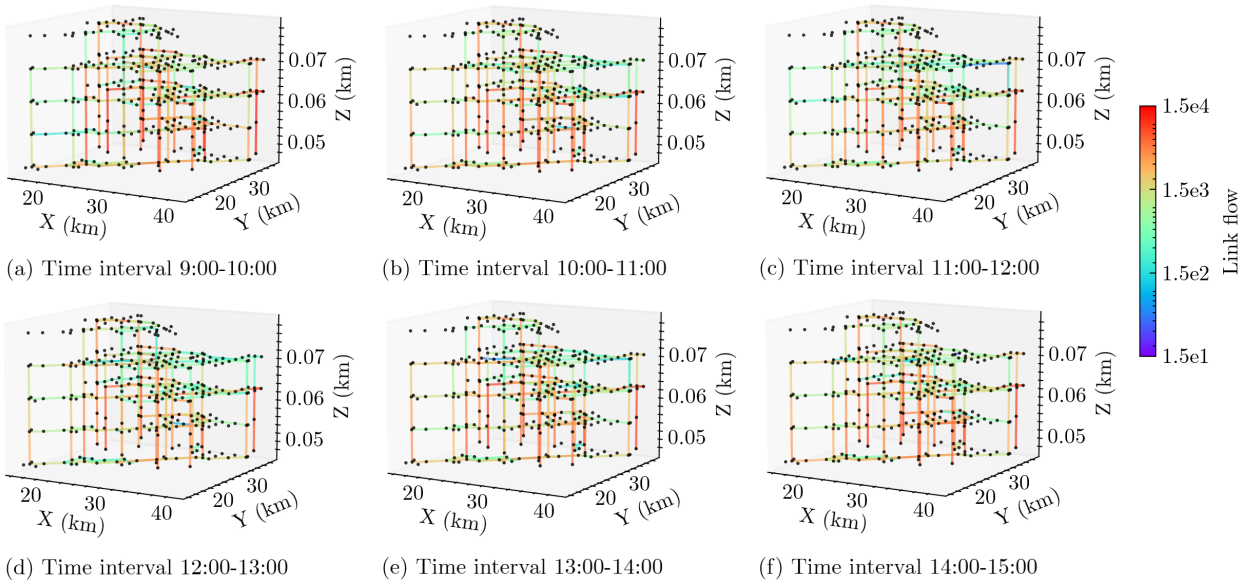

(a) Time interval 9:00-10:00 (b) Time interval 10:00-11:00 (c) Time interval 11:00-12:00

(d) Time interval 12:00-13:00 (e) Time interval 13:00-14:00 (f) Time interval 14:00-15:00

Figure 15: Initial link flow distribution across various time intervals in the UAM route network.

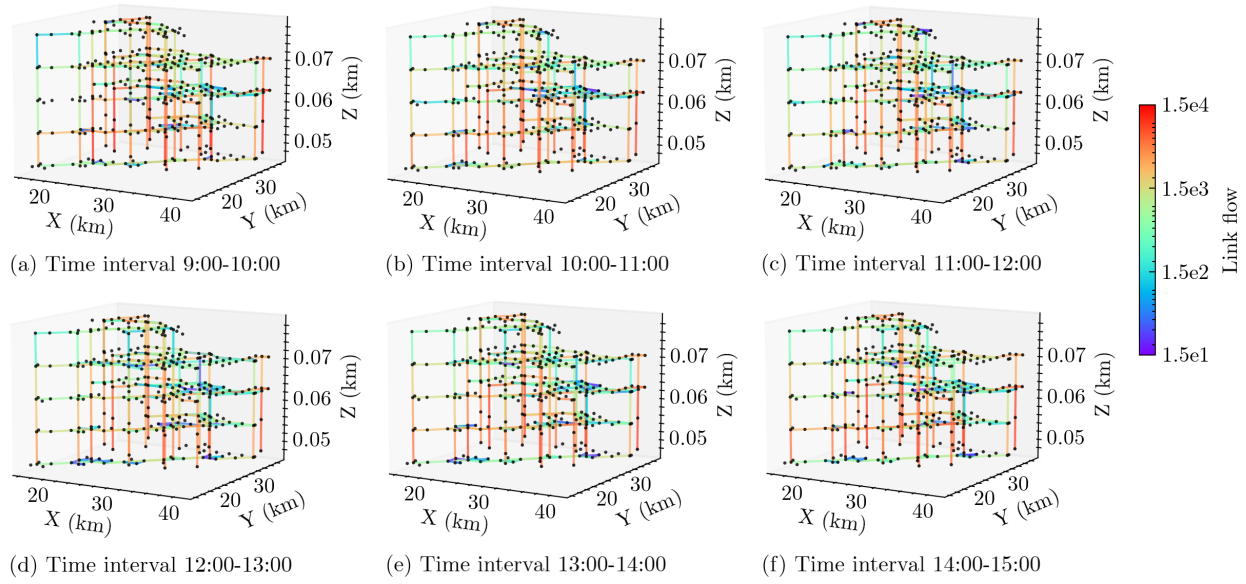

(a) Time interval 9:00-10:00 (b) Time interval 10:00-11:00 (c) Time interval 11:00-12:00

(d) Time interval 12:00-13:00 (e) Time interval 13:00-14:00 (f) Time interval 14:00-15:00

Figure 16: Optimized link flow distribution in the UAM route network across different time intervals.

5. Discussion and conclusions

To tackle the time-varying demand of dense UAM operations in the near future, we formulate a macroscopic QATA model within a centralized strategic planning scheme. This model seeks to efficiently allocate and organize traffic flows on routes within the UAM route network over the planning horizon, with the goal of alleviating congestion and reducing air traffic complexity.

Firstly, the UAM route network is characterized as a directed graph. Air routes are represented as volume segments. Vertiports, delivery stations, and waypoints are modeled as nodes. We then configure the QATA as an optimization problem that considers constrained capacity, propagation of traffic flow, and

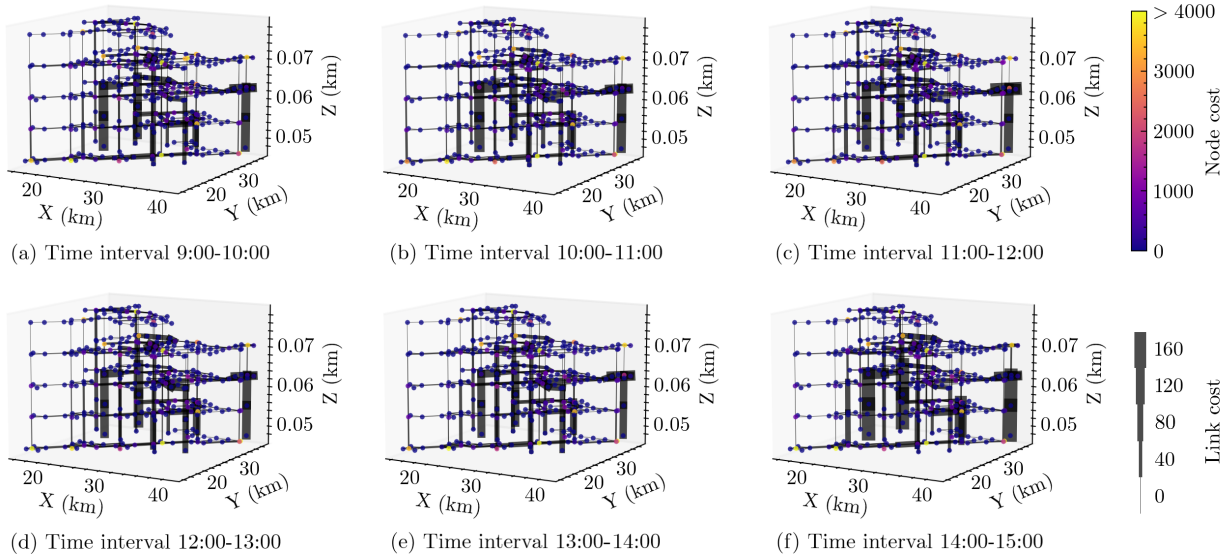

(a) Time interval 9:00-10:00 (b) Time interval 10:00-11:00 (c) Time interval 11:00-12:00

(d) Time interval 12:00-13:00 (e) Time interval 13:00-14:00 (f) Time interval 14:00-15:00

Figure 17: Representation of the initial air traffic complexity and congestion respectively on nodes and links of the UAM route network across various time intervals.

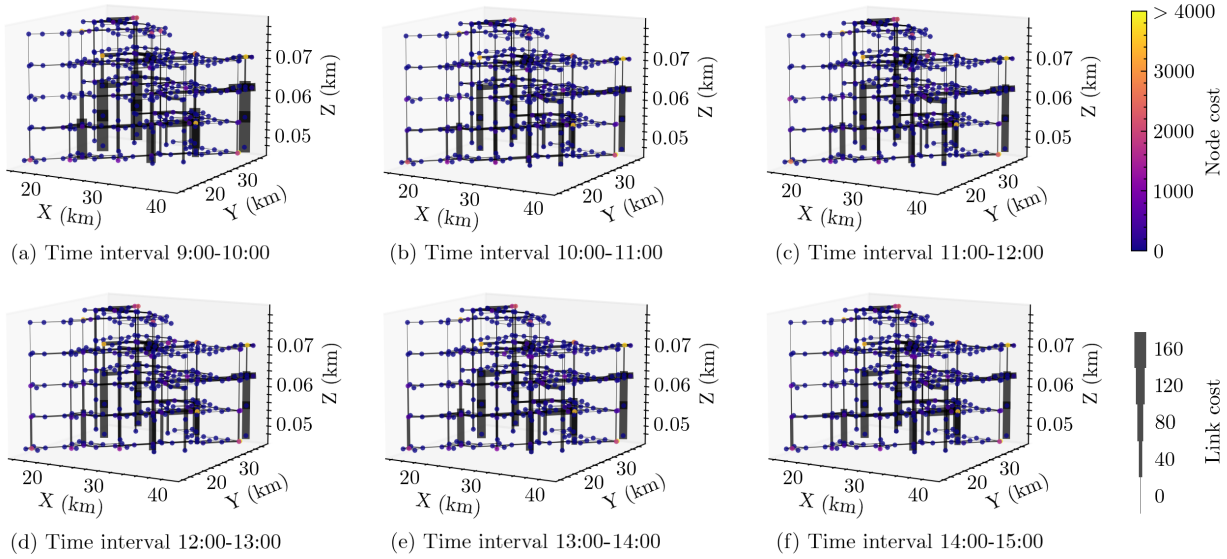

(a) Time interval 9:00-10:00 (b) Time interval 10:00-11:00 (c) Time interval 11:00-12:00

(d) Time interval 12:00-13:00 (e) Time interval 13:00-14:00 (f) Time interval 14:00-15:00

Figure 18: Representation of air traffic complexity and congestion optimized by the proposed model respectively on nodes and links of the UAM route network across various time intervals.

time-varying demand. The objective function involves complexity cost based on the LDS and congestion cost based on energy consumption and traffic density.

In order to solve this problem, a simulation-based rolling horizon framework is proposed to decompose the QATA problem into sub-problems for each time interval. To overcome the limitations inherent in traditional traffic assignment algorithms, we propose the PSA as the optimization algorithm, which is a metaheuristic algorithm that employs parallel computing and a novel neighborhood generation strategy.

Experiments are conducted on a previously designed large-scale UAM route network for a high-density parcel delivery scenario in Singapore's urban airspace. The results in terms of parallelization performance, algorithmic comparison, path flow allocation, link flow allocation, and complexity and congestion costs in

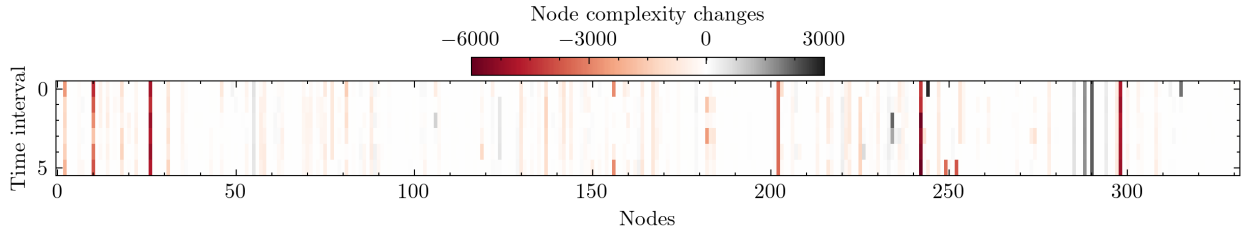

Figure 19: Dynamic variations in complexity costs per node from initial to optimized flow patterns.

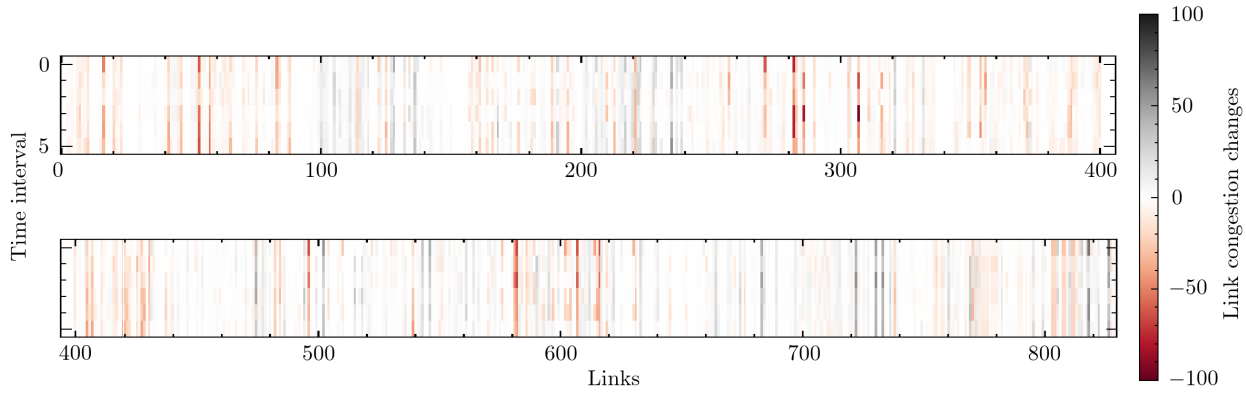

Figure 20: Dynamic variations in congestion costs per link from initial to optimized flow patterns.

network representation, demonstrate that our model can efficiently reduce congestion and air traffic complexity to satisfactory levels. Furthermore, the paths are sufficiently utilized and the flows are intelligently allocated.

In addition to the theoretical significance of this study, our proposed framework can also assist or provide advisories to ATC authorities and ANSP in addressing a series of problems, such as unmanned air traffic flow management, air traffic assignment, UAM traffic flow analysis, Urban airspace complexity measurement, and UAM route network evaluation.

5.1. Limitations and future research

Nevertheless, there exist certain constraints and shortcomings within this paper. Although centralized UTM systems offer significant benefits, as the current UTM concepts highly rely on private-public partnerships where the role of ATM is given to private PSU or UAS Service Supplier (USS), it is not guaranteed nor clear that such private organizations would be incentivized to share information in a way conducive to centralized UTM. In future research, the focus will be on exploring the safe and efficient operation of UAM in a federated scenario that involves a mix of entities or traffic, assuming that the technology in that period will meet a higher level of maturity for UAM.

Another interesting area of future research lies in the integration of the Lagrangian perspective within our existing framework. A microscopic optimization model for managing individual flights can be performed based on the results obtained from the QATA model. It has the potential to yield more optimal solutions and enhance computational efficiency for classic air traffic flow management problems.

6. Acknowledgement

We extend our sincere thanks to PhD candidate Shulu Chen and Associate Professor Peng Wei from George Washington University for their valuable insights into the microscopic simulation of UAM operations. We also thank the anonymous reviewers for their constructive comments and suggestions. This work is

partially supported by the research project CONCORDE of the Defense Innovation Agency (AID) of the French Ministry of Defense (2019650090004707501).

Appendix A. Weighted minimum mean square error estimation of linear dynamical system

In order to transform equation (19) representing a LDS into matrix forms, we can rewrite the LDS as:

$$\mathbf{V} = \mathbf{C}\mathbf{X} \tag{A.1}$$

In the case of this paper,

$$\mathbf{X} = \begin{bmatrix} \sqrt{\omega_1}x_1 & \sqrt{\omega_2}x_2 & \cdots & \sqrt{\omega_N}x_N \\ \sqrt{\omega_1}y_1 & \sqrt{\omega_2}y_2 & \cdots & \sqrt{\omega_N}y_N \\ \sqrt{\omega_1}z_1 & \sqrt{\omega_2}z_2 & \cdots & \sqrt{\omega_N}z_N \\ \sqrt{\omega_1} & \sqrt{\omega_2} & \cdots & \sqrt{\omega_N} \end{bmatrix} \tag{A.2}$$

$$\mathbf{V} = \begin{bmatrix} \sqrt{\omega_1}v_{x,1} & \sqrt{\omega_2}v_{x,2} & \cdots & \sqrt{\omega_N}v_{x,N} \\ \sqrt{\omega_1}v_{y,1} & \sqrt{\omega_2}v_{y,2} & \cdots & \sqrt{\omega_N}v_{y,N} \\ \sqrt{\omega_1}v_{z,1} & \sqrt{\omega_2}v_{z,2} & \cdots & \sqrt{\omega_N}v_{z,N} \end{bmatrix} \tag{A.3}$$

$$\mathbf{C} = \begin{bmatrix} \mathbf{A} \mid \mathbf{b} \end{bmatrix} \tag{A.4}$$

$$\mathbf{A} = \begin{bmatrix} a_{11} & a_{12} & a_{13} \\ a_{21} & a_{22} & a_{23} \\ a_{31} & a_{32} & a_{33} \end{bmatrix} \tag{A.5}$$

$$\mathbf{b} = \begin{bmatrix} b_1 & b_2 & b_3 \end{bmatrix}^\top \tag{A.6}$$

and N is the number of observations.

If the dimension of a LDS is $D_{\text{LDS}} \in \mathbb{N}^+$, then $\mathbf{V} \in \mathbb{R}^{D_{\text{LDS}} \times N}$, $\mathbf{X} \in \mathbb{R}^{D_{\text{LDS}}+1 \times N}$, and $\mathbf{C} \in \mathbb{R}^{D_{\text{LDS}} \times D_{\text{LDS}}+1}$. The error criterion E can be reformulated as

$$E = \|\mathbf{V} - \mathbf{C}\mathbf{X}\|_{\text{F}}^2 \tag{A.7}$$

where $\|\|_{\text{F}}$ represents the Frobenius norm.

The WMMSE aims to find the matrix $\hat{\mathbf{C}}$ that minimizes the error criterion:

$$\hat{\mathbf{C}} = \underset{\mathbf{C} \in \mathbb{R}^{D_{\text{LDS}} \times D_{\text{LDS}}+1}}{\arg\min} E \tag{A.8}$$

To this end, the gradient of E^2 is calculated as:

$$\nabla_{\mathbf{C}} E = -2\left(\mathbf{V} - \mathbf{C}\mathbf{X}\right)\mathbf{X}^\top \tag{A.9}$$

$\nabla_{\mathbf{C}} E = 0$ allow us to calculate $\hat{\mathbf{C}}$. If $\mathbf{X}\mathbf{X}^\top$ is invertible, namely the columns of $\mathbf{X}$ are linearly independent, the LDS problem has a unique solution:

$$\hat{\mathbf{C}} = \mathbf{V}\mathbf{X}^+ \tag{A.10}$$

where $\mathbf{X}^+$ is the pseudo-inverse of $\mathbf{X}$:

$$\mathbf{X}^+ = \mathbf{X}^\top(\mathbf{X}\mathbf{X}^\top)^{-1} \tag{A.11}$$

The matrix $\mathbf{X}$ may not be full-rank or the LDS could be ill-conditioned in some rare cases. To avoid numerical problems associated with the determinant when inversing the matrix $\mathbf{X}\mathbf{X}^\top$, Singular Value Decomposition (SVD) was proposed to solve this problem. $\mathbf{X}$ can be decomposed as:

$$\mathbf{X} = \mathbf{L}\mathbf{\Sigma}\mathbf{R}^\top \tag{A.12}$$

where $\mathbf{L} \in \mathbb{R}^{D_{\text{LDS}}+1 \times D_{\text{LDS}}+1}$ and $\mathbf{R} \in \mathbb{R}^{N \times N}$ are unitary matrices. $\mathbf{L}$ and $\mathbf{R}$ are not unique, which can be composed respectively by the eigenvectors of $\mathbf{X}\mathbf{X}^\top$ and $\mathbf{X}^\top\mathbf{X}$. $\mathbf{\Sigma} \in \mathbb{R}^{D_{\text{LDS}}+1 \times N}$ is a rectangular diagonal matrix with non-negative values on the diagonal.

$\mathbf{X}\mathbf{X}^\top \in \mathbb{R}^{D_{\text{LDS}}+1 \times D_{\text{LDS}}+1}$ is a symmetric matrix, and the square roots of its eigenvalues are the singular values of $\mathbf{X}$. The singular values of $\mathbf{X}$ can be sorted in descending order: $\sigma_1 \geq \sigma_2 \geq \cdots \geq \sigma_r$, where r is the rank of $\mathbf{X}$ and $r \leq \min(D_{\text{LDS}} + 1, N)$. Then, $\mathbf{\Sigma}$ is then defined as:

$$\mathbf{\Sigma} = \left[\begin{array}{cccc:ccc} \sigma_1 & 0 & \cdots & 0 & 0 & \cdots & 0 \\ 0 & \sigma_2 & \cdots & 0 & 0 & \cdots & 0 \\ \vdots & \vdots & \ddots & \vdots & \vdots & \ddots & \vdots \\ 0 & 0 & \cdots & \sigma_r & 0 & \cdots & 0 \\ \hdashline 0 & 0 & \cdots & 0 & 0 & \cdots & 0 \\ \vdots & \vdots & \ddots & \vdots & \vdots & \ddots & \vdots \\ 0 & 0 & \cdots & 0 & 0 & \cdots & 0 \end{array}\right] \begin{array}{l} \\ \\ \\ \\ \left.\begin{array}{l}\\ \\ \\ \end{array}\right\} D_{\text{LDS}} + 1 - r \\ \\ \\ \end{array} \\ \underbrace{\qquad\qquad\qquad}_{N-r} \tag{A.13}$$

where the elements of the last $N - r$ columns and $D_{\text{LDS}} + 1 - r$ rows are 0.

According to Equation (A.12), $\mathbf{X}^+$ can be formulated as :

$$\mathbf{X}^+ = \mathbf{R}\mathbf{\Sigma}^+\mathbf{L}^\top \tag{A.14}$$

where $\mathbf{R} \in \mathbb{R}^{N \times N}$, $\mathbf{L}^T \in \mathbb{R}^{D_{\text{LDS}}+1 \times D_{\text{LDS}}+1}$. $\mathbf{\Sigma}^+ \in \mathbb{R}^{N \times D_{\text{LDS}}+1}$ can be formulated as:

$$\mathbf{\Sigma}^+ = \left[\begin{array}{cccc:ccc} \frac{1}{\sigma_1} & 0 & \cdots & 0 & 0 & \cdots & 0 \\ 0 & \frac{1}{\sigma_2} & \cdots & 0 & 0 & \cdots & 0 \\ \vdots & \vdots & \ddots & \vdots & \vdots & \ddots & \vdots \\ 0 & 0 & \cdots & \frac{1}{\sigma_r} & 0 & \cdots & 0 \\ \hdashline 0 & 0 & \cdots & 0 & 0 & \cdots & 0 \\ \vdots & \vdots & \ddots & \vdots & \vdots & \ddots & \vdots \\ 0 & 0 & \cdots & 0 & 0 & \cdots & 0 \end{array}\right] \begin{array}{l} \\ \\ \\ \\ \left.\begin{array}{l}\\ \\ \\ \end{array}\right\} N - r \\ \\ \\ \end{array} \\ \underbrace{\qquad\qquad\qquad}_{D_{\text{LDS}}+1-r} \tag{A.15}$$

where the elements of the last $D_{\text{LDS}} + 1 - r$ columns and $N - r$ rows are 0.

$\hat{\mathbf{C}}$ is thus given by:

$$\hat{\mathbf{C}} = \mathbf{V}\mathbf{R}\mathbf{\Sigma}^+\mathbf{L}^\top \tag{A.16}$$

Finally, $\hat{\mathbf{A}}$ can be extracted from $\hat{\mathbf{C}}$ according to Equation (A.4).

Appendix B. Representative conventional algorithms for dynamic traffic assignment

Appendix B.1. Dafermos' algorithm

Dafermos' Algorithm (DA) is a widely used sequential decomposition algorithm for traffic assignment problems (Dafermos and Sparrow, 1969, Dafermos, 1971, 1972). In the inner loop of each time interval k, DA successively optimizes on each OD w to decompose the problem into a sequence of simpler ones. Starting from an initial flow pattern, the global cost function converges by transferring flow from the most expensive path $p_{w,\max}$ to the least expensive path $p_{w,\min}$ in terms of the marginal cost C'_p, where

$$p_{w,\min} = \arg\min_{p \in \mathcal{P}_w} C'_p \tag{B.1}$$

$$p_{w,\max} = \arg\max_{p \in \mathcal{P}_w, F_p > 0} C'_p \tag{B.2}$$

and

$$C'_p(\boldsymbol{f}) = \frac{\partial \mathscr{C}}{\partial F_p} \tag{B.3}$$

In our problem, the dominant eigenvalue of the LDS involved in the cost function is also dependent on the path flows. Thus, the derivative of the cost function does not have an analytical form. We use numerical differentiation to estimate the marginal cost:

$$\frac{\partial \mathscr{C}}{\partial F_p} = \lim_{\varepsilon \to 0} \frac{\mathscr{C}(F_p + \varepsilon) - \mathscr{C}(F_p)}{\varepsilon} \tag{B.4}$$

New path flow pattern $\hat{\boldsymbol{F}}_w$ is updated using the following rule:

$$\begin{cases} \hat{F}_p = F_p, \quad \forall p \in (\mathcal{P}_w - \{p_{w,\min}, p_{w,\max}\}) \\ \hat{F}_{p_{w,\min}} = F_{p_{w,\min}} + \sigma_w \\ \hat{F}_{p_{w,\max}} = F_{p_{w,\max}} - \sigma_w \end{cases} \tag{B.5}$$

where σ_w is the solution in $[-F_{p_{w,\min}}, F_{p_{w,\max}}]$ that minimizes $\mathscr{C}$ and satisfies the constraints. To facilitate the computation, σ_w is selected from a set of size N_d uniformly discretized from interval $[-F_{p_{w,\min}}, F_{p_{w,\max}}]$.

Appendix B.2. Probabilistic method

The Probabilistic Method (PM) (Ameli et al., 2020b) is a trip-based algorithm based on the swapping probabilities. In iteration i, a fraction of $1/(i+1)$ of vehicles on non-least-cost paths swaps to the path with the minimum cost. For each path p in OD w in time interval k, the swapping probability is given by the following formula:

$$\Pr(p_{\text{swap}} = 1) = \frac{\mathscr{C}_{p,k} - \min_{p \in P_w}(\mathscr{C}_{p,k})}{\mathscr{C}_{p,k}} \tag{B.6}$$

where p_{swap} is a binary decision variable for swapping.

This algorithm does not require step size information. Furthermore, the ranking process can be avoided.

References

FAA. FAA Aerospace Forecast Fiscal Years 2022–2042, 2020a. URL `https://www.faa.gov/sites/faa.gov/files/2022-06/FY2022_42_FAA_Aerospace_Forecast.pdf`. Accessed: 31/08/2022.

Shulu Chen, Peng Wei, Antony D Evans, and Maxim Egorov. Estimating airspace resource capacity for advanced air mobility operations. In *AIAA AVIATION 2022 Forum*, page 3317, 2022.

Karthik Balakrishnan, Joe Polastre, Jessie Mooberry, Richard Golding, and Peter Sachs. Blueprint for the sky: The roadmap for the safe integration of autonomous aircraft. *Airbus UTM, San Francisco, CA*, 2018.

Malik Doole, Joost Ellerbroek, and Jacco Hoekstra. Estimation of traffic density from drone-based delivery in very low level urban airspace. *Journal of Air Transport Management*, 88:101862, 2020.

Shiva Ram Reddy Singireddy and Tugrul U. Daim. Technology roadmap: Drone delivery – amazon prime air. In *Innovation, Technology, and Knowledge Management*, pages 387–412. Springer International Publishing, 2018. doi: 10.1007/978-3-319-68987-6_13.

Brock Lascara, Andrew Lacher, Matthew DeGarmo, David Maroney, Rick Niles, and Lakshmi Vempati. Urban air mobility airspace integration concepts. Technical report, The MITRE Corporation, 2019.

KH Low, Lu Gan, and Shixin Mao. A preliminary study in managing safe and efficient low-altitude unmanned aircraft system operations in a densely built-up urban environment. *Air Traffic Management Research Institute, School of Mechanical and Aerospace Engineering Nanyang Technological University*, 2014.

Malik Doole, Joost Ellerbroek, Victor L Knoop, and Jacco M Hoekstra. Constrained urban airspace design for large-scale drone-based delivery traffic. *Aerospace*, 8(2):38, 2021.

FAA. Concepts of operations v2.0, foundational principles, roles and responsibilities, scenarios and operational threads. Technical report, U.S. department of transportation, 2020b.

Dae-Sung Jang, Corey A. Ippolito, Shankar Sankararaman, and Vahram Stepanyan. Concepts of airspace structures and system analysis for UAS traffic flows for urban areas. In *AIAA Information Systems-AIAA Infotech @ Aerospace*. American Institute of Aeronautics and Astronautics, jan 2017. doi: 10.2514/6.2017-0449. URL `https://doi.org/10.2514%2F6.2017-0449`.

Dagi Geister. Concept for Urban Airspace Integration DLR U-Space Blueprint. Technical report, Institute of Flight Guidance, 2017.

Emmanuel Sunil, JM Hoekstra, Joost Ellerbroek, Frank Bussink, Dennis Nieuwenhuisen, Andrija Vidosavljevic, and Stefan Kern. Metropolis: Relating airspace structure and capacity for extreme traffic densities. In *Proceedings of the 11th USA/Europe Air Traffic Management Research and Development Seminar (ATM2015), Lisbon (Portugal), 23-26 June, 2015*. FAA/Eurocontrol, 2015.

Aleksandar Bauranov and Jasenka Rakas. Designing airspace for urban air mobility: A review of concepts and approaches. *Progress in Aerospace Sciences*, 125:100726, aug 2021. doi: 10.1016/j.paerosci.2021.100726. URL `https://doi.org/10.1016%2Fj.paerosci.2021.100726`.

Brian P Hill, Dwight DeCarme, Matt Metcalfe, Christine Griffin, Sterling Wiggins, Chris Metts, Bill Bastedo, Michael D Patterson, and Nancy L Mendonca. Uam vision concept of operations (conops) uam maturity level (uml) 4. 2020.

Antony D Evans, Maxim Egorov, and Scot Campbell. Accommodating operational uncertainty in urban air mobility operations with strategic deconfliction. In *AIAA AVIATION 2021 FORUM*, page 2333, 2021.

Hok Kwan Ng. Strategic planning with unscented optimal guidance for urban air mobility. In *AIAA AVIATION 2020 FORUM*, page 2904, 2020.

Xiang Yu and Youmin Zhang. Sense and avoid technologies with applications to unmanned aircraft systems: Review and prospects. *Progress in Aerospace Sciences*, 74:152–166, 2015.

Michael D Patterson, Douglas R Isaacson, Nancy L Mendonca, Natasha A Neogi, Kenneth H Goodrich, Matt Metcalfe, Bill Bastedo, Chris Metts, Brian P Hill, Dwight DeCarme, et al. An initial concept for intermediate-state, passenger-carrying urban air mobility operations. In *AIAA Scitech 2021 Forum*, page 1626, 2021.

Thomas Prevot, Joseph Rios, Parimal Kopardekar, John E Robinson III, Marcus Johnson, and Jaewoo Jung. Uas traffic management (utm) concept of operations to safely enable low altitude flight operations. In *16th AIAA Aviation Technology, Integration, and Operations Conference*, page 3292, 2016.

Kenneth H Goodrich and Bryan Barmore. Exploratory analysis of the airspace throughput and sensitivities of an urban air mobility system. In *2018 Aviation Technology, Integration, and Operations Conference*, page 3364, 2018.

Daniel Delahaye and Stéphane Puechmorel. *Modeling and optimization of air traffic*. John Wiley & Sons, 2013a.

Allen R Ferguson and George B Dantzig. The problem of routing aircraft: A mathematical solution. Technical report, RAND PROJECT AIR FORCE ARLINGTON VA, 1954.

Jean-Loup Farges and Daniel Delahaye. Pricing Policies for Air Traffic Assignment. *Air Transportation Systems Engineering*, pages 143–157, 2001. doi: 10.2514/5.9781600866630.0143.0157.

Karine Deschinkel, Jean-Loup Farges, and Daniel Delahaye. Optimizing and assigning price levels for air traffic management. *Transportation Research Part E: Logistics and Transportation Review*, 38(3-4):221–237, 2002. doi: 10.1016/s1366-5545(02)00007-8.

Daniel Delahaye, Oussedik Sofiane, and Stephane Puechmorel. Airspace congestion smoothing by multi-objective genetic algorithm. In *Proceedings of the 2005 ACM symposium on Applied computing - SAC '05*, pages 907–912. ACM Press, 2005. doi: 10.1145/1066677.1066887.

Jenaro Nosedal, Miquel A Piera, Sergio Ruiz, and Alvaro Nosedal. An efficient algorithm for smoothing airspace congestion by fine-tuning take-off times. *Transportation Research Part C: Emerging Technologies*, 44:171–184, 2014. doi: 10.1016/j.trc.2014.03.017.

Issam Strub and Alexandre Bayen. Optimal control of air traffic networks using continuous flow models. In *AIAA Guidance, Navigation, and Control Conference and Exhibit*, page 6228. American Institute of Aeronautics and Astronautics, 2006. doi: 10.2514/6.2006-6228.

Dimitris Bertsimas, Guglielmo Lulli, and Amedeo Odoni. An Integer Optimization Approach to Large-Scale Air Traffic Flow Management. *Operations Research*, 59(1):211–227, 2011. doi: 10.1287/opre.1100.0899.

Miao Zhang, Kai-quan Cai, and Yan-bo Zhu. An improved multi-objective particle swarm optimizer for air traffic flow network rerouting problem. In *2012 IEEE/AIAA 31st Digital Avionics Systems Conference (DASC)*, pages 4B4—-1. IEEE, 2012. doi: 10.1109/dasc.2012.6382335.

Xuejun Zhang, Xiangmin Guan, Yanbo Zhu, and Jiaxing Lei. Strategic flight assignment approach based on multi-objective

parallel evolution algorithm with dynamic migration interval. *Chinese Journal of Aeronautics*, 28(2):556–563, 2015. doi: 10.1016/j.cja.2015.01.012.

Daniel Delahaye and Stéphane Puechmorel. Genetic Algorithms and Improvements. In *Modeling and Optimization of Air Traffic*, pages 37–66. John Wiley & Sons, Inc., 2013b. doi: 10.1002/9781118743805.ch2.

Mohamed Haouari, Najla Aissaoui, and Farah Zeghal Mansour. Network flow-based approaches for integrated aircraft fleeting and routing. *European Journal of Operational Research*, 193(2):591–599, 2009. doi: 10.1016/j.ejor.2007.11.042.

Fedja T Netjasov. A model of air traffic assignment as a measure for mitigating noise at airports: The Zurich Airport Case. *Transportation Planning and Technology*, 31(5):487–508, 2008. doi: 10.1080/03081060802364448.

Emir Ganić, Obrad Babić, Mirjana Čangalović, and Milan Stanojević. Air traffic assignment to reduce population noise exposure using activity-based approach. *Transportation Research Part D: Transport and Environment*, 63:58–71, 2018.

Paul Chatelain and Mathieu Van Vyve. Modeling fair air traffic assignment in the vicinity of airports. *Transportation Research Part D: Transport and Environment*, 65:213–228, 2018. ISSN 13619209. doi: 10.1016/j.trd.2018.08.016. URL `https://doi.org/10.1016/j.trd.2018.08.016`.

Vinh Ho-Huu, Emir Ganić, Sander Hartjes, Obrad Babić, and Richard Curran. Air traffic assignment based on daily population mobility to reduce aircraft noise effects and fuel consumption. *Transportation Research Part D: Transport and Environment*, 72:127–147, 2019. doi: 10.1016/j.trd.2019.04.007.

J T Economou, G Kladis, A Tsourdos, and B A White. UAV optimum energy assignment using Dijkstra's Algorithm. In *2007 European Control Conference (ECC)*, pages 287–292. IEEE, 2007.

Petar Mirosavljević, Slobodan Gvozdenović, and Olja Čokorilo. A model of air traffic assignment as part of airport air pollution management system. *Aviation*, 15(4):92–100, 2011. ISSN 16487788. doi: 10.3846/16487788.2011.651792.

Xiaowei Jiang, Qiang Zhou, and Ying Ye. Method of task assignment for UAV based on particle swarm optimization in logistics. In *Proceedings of the 2017 International Conference on Intelligent Systems, Metaheuristics & Swarm Intelligence*, pages 113–117, 2017.

Zhenyu Zhou, Junhao Feng, Bo Gu, Bo Ai, Shahid Mumtaz, Jonathan Rodriguez, and Mohsen Guizani. When mobile crowd sensing meets UAV: Energy-efficient task assignment and route planning. *IEEE Transactions on Communications*, 66(11): 5526–5538, 2018.

Linhui Cheng, Luo Zhong, Shasha Tian, and Jiaxu Xing. Task Assignment Algorithm for Road Patrol by Multiple UAVs With Multiple Bases and Rechargeable Endurance. *IEEE Access*, 7:144381–144397, 2019.

Dianxiong Liu, Jinlong Wang, Kun Xu, Yuhua Xu, Yang Yang, Yitao Xu, Qihui Wu, and Alagan Anpalagan. Task-driven relay assignment in distributed UAV communication networks. *IEEE Transactions on Vehicular Technology*, 68(11):11003–11017, 2019.

Alessandro Bombelli. *Strategic Air Traffic Planning Using Eulerian Route Based Modeling and Optimization*. University of California, Irvine, 2017.

Stéphane Mollier, Maria Laura Delle Monache, Carlos Canudas-de Wit, and Benjamin Seibold. Two-dimensional macroscopic model for large scale traffic networks. *Transportation Research Part B: Methodological*, 122:309–326, 2019.

Maria Prandini, Luigi Piroddi, Stephane Puechmorel, and Silvie Luisa Brazdilova. Toward air traffic complexity assessment in new generation air traffic management systems. *IEEE transactions on intelligent transportation systems*, 12(3):809–818, 2011.

Daniel Delahaye and Stéphane Puechmorel. Air traffic complexity: towards intrinsic metrics. In *Proceedings of the third USA/Europe Air Traffic Management R & D Seminar*, 2000.

Jonathan M Histon, R John Hansman, Guillaume Aigoin, Daniel Delahaye, and Stephane Puechmorel. Introducing structural considerations into complexity metrics. *Air Traffic Control Quarterly*, 10(2):115–130, 2002. doi: 10.2514/atcq.10.2.115.

Thimjo Koca, Miquel Angel Piera, and Marko Radanovic. A methodology to perform air traffic complexity analysis based on spatio-temporal regions constructed around aircraft conflicts. *IEEE Access*, 7:104528–104541, 2019.

Daniel Delahaye and Stéphane Puechmorel. Modeling and Optimization of Air Traffic. *Modeling and Optimization of Air Traffic*, pages 1–329, 2013c. doi: 10.1002/9781118743805.

Hanno Essén. Average angular velocity. *European Journal of Physics*, 14(5):201–205, 1993. doi: 10.1088/0143-0807/14/5/002.

D Delahaye, P Paimblanc, S Puechmorel, J M Histon, and R J Hansman. A new air traffic complexity metric based on dynamical system modelization. In *Proceedings. The 21st Digital Avionics Systems Conference*, volume 1, pages 4A2—-4A2. IEEE, 2002. doi: 10.1109/dasc.2002.1067960.

Paveen Juntama, Supatcha Chaimatanan, Sameer Alam, and Daniel Delahaye. A distributed metaheuristic approach for complexity reduction in air traffic for strategic 4d trajectory optimization. In *2020 International Conference on Artificial Intelligence and Data Analytics for Air Transportation (AIDA-AT)*, pages 1–9. IEEE, 2020. doi: 10.1109/aida-at48540.2020.9049200.

Marko Radanovic, Miquel Angel Piera Eroles, Thimjo Koca, and Juan Jose Ramos Gonzalez. Surrounding traffic complexity analysis for efficient and stable conflict resolution. *Transportation research part C: emerging technologies*, 95:105–124, 2018.

Ralvi Isufaj, Marsel Omeri, Miquel Angel Piera, Jaume Saez Valls, and Christian Eduardo Verdonk Gallego. From single aircraft to communities: A neutral interpretation of air traffic complexity dynamics. *arXiv preprint arXiv:2208.01740*, 2022.

Keumjin Lee, Eric Feron, and Amy Pritchett. Air traffic complexity: an input-output approach. In *2007 American Control Conference*, pages 474–479. IEEE, 2007.

Minghua Zhang, Hua Xie, Dongfang Zhang, Jiaming Ge, and Haiyan Chen. Handling label noise in air traffic complexity evaluation based on confident learning and xgboost. *Transactions of Nanjing University of Aeronautics & Astronautics*, 37 (6):936–946, 2021.

Daniel Delahaye, Stephane Puechmorel, John Hansman, and Jonathan Histon. Air traffic complexity map based on non linear dynamical systems. *Air Traffic Control Quarterly*, 12(4):367–388, 2004. doi: 10.2514/atcq.12.4.367.

Daniel Delahaye and Stephane Puechmorel. Air traffic complexity based on dynamical systems. In *49th IEEE Conference on Decision and Control (CDC)*. IEEE, 2010. doi: 10.1109/cdc.2010.5718004.

Tambet Treimuth, Daniel Delahaye, Stephane Puechmorel, and Sandra Ulrich Ngueveu. Parallel complexity computation based on dynamical systems. In *2015 IEEE/AIAA 34th Digital Avionics Systems Conference (DASC)*, pages 1C2—-1. IEEE, 2015. doi: 10.1109/dasc.2015.7311340.

Paveen Juntama, Daniel Delahaye, Supatcha Chaimatanan, and Sameer Alam. Hyperheuristic approach based on reinforcement learning for air traffic complexity mitigation. *Journal of Aerospace Information Systems*, pages 1–16, 2022.

Yi-Chang Chiu, Jon Bottom, Michael Mahut, Alexander Paz, Ramachandran Balakrishna, Steven Waller, and Jim Hicks. *Dynamic traffic assignment: A primer (Transportation Research Circular E-C153)*. Transportation Research Circular. Transportation Research Board, United States of America, 2011. URL `https://eprints.qut.edu.au/133232/`.

Mostafa Ameli, Jean-Patrick Lebacque, and Ludovic Leclercq. Simulation-based dynamic traffic assignment: Meta-heuristic solution methods with parallel computing. *Computer-Aided Civil and Infrastructure Engineering*, 35(10):1047–1062, 2020a.

Zhengyi Wang, Daniel Delahaye, Jean-Loup Farges, and Alam Sameer. Air Traffic Assignment for Intensive Urban Air Mobility Operations. *Journal of Aerospace Information Systems*, In press(-):1–16, 2021.

Zhengyi Wang, Daniel Delahaye, Jean-Loup Farges, and Sameer Alam. Route network design in low-altitude airspace for future urban air mobility operations A case study of urban airspace of Singapore. In *10th International Conference on Research in Air Transportation*, TAMPA, United States, June 2022a. URL `https://hal-enac.archives-ouvertes.fr/hal-03701655`.

Zhengyi Wang, Daniel Delahaye, Jean-Loup Farges, and Sameer Alam. Complexity optimal air traffic assignment in multi-layer transport network for urban air mobility operations. *Transportation Research Part C: Emerging Technologies*, 142:103776, 2022b.

Michael Patriksson. *The traffic assignment problem: models and methods*. Courier Dover Publications, 2015.

Kenneth H Goodrich and Colin R Theodore. Description of the nasa urban air mobility maturity level (uml) scale. In *AIAA Scitech 2021 Forum*, page 1627, 2021.

Christopher Decker and Paul Chiambaretto. Economic policy choices and trade-offs for unmanned aircraft systems traffic management (utm): Insights from europe and the united states. *Transportation research part A: policy and practice*, 157: 40–58, 2022.

Daniel Delahaye. *Optimisation de la sectorisation de l'espace aérien par algorithmes génétiques*. PhD thesis, Toulouse, ENSAE, 1995.

Daniel Delahaye, Adrían García, Julien Lavandier, Supatcha Chaimatanan, and Manuel Soler. Air traffic complexity map based on linear dynamical systems. *Aerospace*, 9(5):230, 2022.

Hiroki Sayama. *Introduction to the modeling and analysis of complex systems*. Open SUNY Textbooks, 2015.

Shulu Chen, Antony Evans, Marc Brittain, and Peng Wei. Integrated conflict management for uam with strategic demand capacity balancing and learning-based tactical deconfliction. *arXiv preprint arXiv:2305.10556*, 2023.

Scott Kirkpatrick, C Daniel Gelatt Jr, and Mario P Vecchi. Optimization by simulated annealing. *science*, 220(4598):671–680, 1983.

Mark Fleischer and Sheldon H Jacobson. Information theory and the finite-time behavior of the simulated annealing algorithm: Experimental results. *INFORMS Journal on Computing*, 11(1):35–43, 1999.

Esin Onbaşoğlu and Linet Özdamar. Parallel simulated annealing algorithms in global optimization. *Journal of global optimization*, 19(1):27–50, 2001.

Nicholas Metropolis, Arianna W. Rosenbluth, Marshall N. Rosenbluth, Augusta H. Teller, and Edward Teller. Equation of state calculations by fast computing machines. Technical report, mar 1953. URL `https://doi.org/10.2172%2F4390578`.

Huiping Liu, Cheqing Jin, Bin Yang, and Aoying Zhou. Finding top-k shortest paths with diversity. *IEEE Transactions on Knowledge and Data Engineering*, 30(3):488–502, 2017.

Jari Saramäki, Mikko Kivelä, Jukka-Pekka Onnela, et al. Generalizations of the clustering coefficient to weighted complex networks. *Physical Review E*, 75(2):027105, 2007.

Mark EJ Newman. Mixing patterns in networks. *Physical review E*, 67(2):026126, 2003.

Lianbo Deng, Junhao Zeng, and Hongda Mei. Passenger flow pushing assignment method for an urban rail network based on hierarchical path and line decomposition. *Sustainability*, 11(22):6441, 2019.

Mostafa Ameli, Jean-Patrick Lebacque, and Ludovic Leclercq. Cross-comparison of convergence algorithms to solve trip-based dynamic traffic assignment problems. *Computer-Aided Civil and Infrastructure Engineering*, 35(3):219–240, 2020b.

Herbert Robbins and Sutton Monro. A stochastic approximation method. *The annals of mathematical statistics*, pages 400–407, 1951.

Chung-Cheng Lu, Hani S Mahmassani, and Xuesong Zhou. Equivalent gap function-based reformulation and solution algorithm for the dynamic user equilibrium problem. *Transportation Research Part B: Methodological*, 43(3):345–364, 2009.

Hayssam Sbayti, Chung-Cheng Lu, and Hani S Mahmassani. Efficient implementation of method of successive averages in simulation-based dynamic traffic assignment models for large-scale network applications. *Transportation Research Record*, 2029(1):22–30, 2007.

Stella C Dafermos and Frederick T Sparrow. The traffic assignment problem for a general network. *Journal of Research of the National Bureau of Standards B*, 73(2):91–118, 1969.

Stella C. Dafermos. An extended traffic assignment model with applications to two-way traffic. *Transportation Science*, 5(4): 366–389, nov 1971. doi: 10.1287/trsc.5.4.366.

Stella C. Dafermos. The traffic assignment problem for multiclass-user transportation networks. *Transportation Science*, 6(1): 73–87, feb 1972. doi: 10.1287/trsc.6.1.73.